

Waves in systems with cross-diffusion as a new class of nonlinear waves

M A Tsyganov, V N Biktashev, J Brindley, A V Holden, G R Ivanitsky

DOI: 10.1070/PU2007v050n03ABEH006114

Contents

1. Introduction	263
2. Nonlinear cross-diffusion. Taxis waves	265
2.1 Taxis in population systems; 2.2 Bacterial population waves; 2.3 Restoration of bacterial population waves during isolation of the inoculation center; 2.4 Soliton-like regime of interaction between bacterial waves	
3. Main properties of population taxis waves	270
3.1 Waves in a reaction–diffusion–taxis system ($\gamma = 0.01$); 3.2 Waves in a reaction–taxis system ($\gamma = 0.016$); 3.3 Mechanisms of the quasi-soliton interaction between taxis waves	
4. Taxis waves in two-dimensional media	274
4.1 Spiral waves; 4.2 Alternative behavior of wavebreaks; 4.3 Partial reflection and self-supporting activity	
5. Half-soliton interactions between population taxis waves	276
5.1 One-dimensional case; 5.2 Two-dimensional medium; 5.3 Taxitons. Dependence of the reflection regime on the taxis wave interaction angle	
6. Waves in excitable media with linear cross-diffusion	278
6.1 Examples of systems with cross-diffusion; 6.2 Characteristic wave properties; 6.3 Quasi-soliton wave interaction	
7. Conclusion	284
References	285

Abstract. Research on spatially extended excitable systems with cross-diffusion components is reviewed. Particular attention is given to the new phenomena of the quasi-soliton and half-soliton interaction of excitation waves, which are specific to such systems and occur along with the standard nonsoliton wave interaction that causes the waves to mutually annihilate. A correlation is shown to exist between interaction regimes and wave profile shapes. One example of a cross-diffusion system is population systems with taxes. Based on the mathematical

models of and experimental work with bacterial populations, waves in excitable cross-diffusion systems can be identified as a new class of nonlinear waves.

1. Introduction

Since the work of Turing [1], the majority of mathematical models simulating the formation and propagation of nonlinear waves and structural self-organization processes in physical, chemical, and social systems have been based on reaction–diffusion systems, where nonlinear terms describe kinetics, while transfer processes are represented by isotropic diffusion [2–9]. But more complicated diffusion mechanisms, such as nonlinear, anisotropic, and cross-diffusion, are of importance in many other systems.

Most authors focus on direct diffusion (self-diffusion) of N components φ_k , $k = 1, \dots, N$, described by the equations

$$\partial_t \varphi_k + \partial_x J_k = F_k(\varphi_j),$$

where the flux $J_k = -D_k \partial_x \varphi_k$ and diffusion coefficients D_k are constants [10]. In this class of systems, formation of spatio-temporal structures is determined by the diffusion coefficients D_k and specific forms of the kinetic functions of reaction processes F_k . The case where diffusion coefficients are not constants but depend on dynamic variables corresponds to nonlinear diffusion. Examples of nonlinear diffusion can be found in mass-transfer processes in porous media and in population models [11, 12]. Mathematical models with diffusion coefficients depending on the bacterial density have been used to describe the formation of complicated spatial

M A Tsyganov, G R Ivanitsky Institute of Theoretical and Experimental Biophysics, Russian Academy of Sciences,
ul. Institutskaya 3, 142290 Pushchino, Moscow region,
Russian Federation

Tel. (7-495) 632 78 69. Fax (7-4967) 33 53 03

E-mail: tsyganov@iteb.ru, ivanitsky@iteb.ru

V N Biktashev Department of Mathematical Sciences,

University of Liverpool, Liverpool L69 7ZL, UK

Tel. +44 (151) 794 40 04. Fax +44 (151) 794 40 61

E-mail: vnb@liv.ac.uk

J Brindley Department of Applied Mathematics, University of Leeds,
Leeds LS2 9JT, UK

Tel. +44 (113) 343 51 34. Fax +44 (113) 343 50 90

E-mail: amtjb@maths.leeds.ac.uk

A V Holden Faculty of Biological Sciences, University of Leeds,

Leeds LS2 9JT, UK

Tel. +44 (113) 233 42 51. Fax +44 (113) 233 42 30

E-mail: a.v.holden@leeds.ac.uk

Received 28 April 2006, revised 18 July 2006

Uspekhi Fizicheskikh Nauk 177 (3) 275–300 (2007)

Translated by Yu V Morozov; edited by A M Semikhatov

structures in growing microbial colonies [13–16]. Regimes with sharpening and spatial localization in open dissipative systems are described by models with nonlinear diffusion [17, 18].

The natural generalization of these systems includes the use of cross-diffusion, for which the flow is written as [10]

$$J_k = - \sum_j D_{kj}(\varphi) \partial_x \varphi_j.$$

Certain cross-diffusion models have been considered in a number of studies in physical (plasma physics) [10, 19], chemical (dynamics of electrolyte solutions) [20], and biological (cross-diffusion transport) [21] systems. The same refers to population dynamics [9, 22–25] and ecological (forest age-structure dynamics) [26, 27] studies. The Burridge–Knopoff model was used to describe interactions between tectonic plates in seismology. Mathematical models with cross-diffusion have been extensively employed in the past decade to gain insight into the mechanisms of tumor growth and development [30–36] (along with reaction–diffusion–advection systems [37]).

To explain what we mean by the term ‘cross-diffusion,’ we consider a system of two partial differential equations in a one-dimensional case:

$$\begin{aligned} \frac{\partial u}{\partial t} &= f(u, v) + D_1 \frac{\partial^2 u}{\partial x^2} + h_1 \frac{\partial}{\partial x} \left(Q_1(u, v) \frac{\partial v}{\partial x} \right), \\ \frac{\partial v}{\partial t} &= g(u, v) + D_2 \frac{\partial^2 v}{\partial x^2} + h_2 \frac{\partial}{\partial x} \left(Q_2(u, v) \frac{\partial u}{\partial x} \right). \end{aligned} \quad (1)$$

At $h_1 = h_2 = 0$, mathematical model (1) is a reaction–diffusion system with the diffusion coefficients $D_1 \geq 0$, $D_2 \geq 0$ (at least one $D_i \neq 0$). When at least one coefficient $h_i \neq 0$ (with any sign), system (1) is of the cross-diffusion type. In linear cross-diffusion, $Q_i(u, v) = \text{const}$ for $i = 1, 2$; in nonlinear cross-diffusion, $Q_i(u, v) \neq \text{const}$ for at least one i .

Cross-diffusion means that the spatial movements of an object described by one of the variables occur due to the diffusion of another object described by a different variable. The simplest example at the population level is a parasite (first object) moving by diffusion of a host (second object). The term ‘self-diffusion’ (diffusion, direct diffusion, ordinary diffusion) implies an individual traveling with the diffusion flow from a high concentration to a low-concentration region. The term cross-diffusion means that a flow/motion of individuals of one species occurs in the gradient of other individuals/substances. Cross-diffusion coefficients may be positive, negative, or zero. A positive coefficient suggests motion towards a region with low concentration of other individuals/substances; a negative coefficient indicates that motion occurs towards a region with a high concentration of other individuals/substances. Systems with cross-diffusion are rather widespread in nature and play an important role, especially in biophysical and biomedical situations.

The ability to spontaneously form and develop ordered dynamic and static structures is one of the properties of reaction–diffusion systems. As a result of self-organization, such systems can acquire properties that were present in none of the constituent components. The formation of spatially and temporally ordered structures is a key issue for understanding the development of various stages of morphogenesis, population and ecosystem dynamics, excitable tissues, neuronal networks, etc. [38–43]. The simplest variants of

morphogenesis are associated with the development of a multicellular ‘organism’ from populations of unicellular organisms, which most often occurs when the populations are under extreme conditions. A similar ability to form complex ordered dynamic and static structures is inherent in cross-diffusion systems. Cross-diffusion must be taken into account in simulating extended predator–prey population systems [9, 24, 25, 44–47]. Cross-diffusion systems play a primary role in mathematical modeling of pigmentation patterns in animals [9, 48–52], the localization and motion of leukocytes in response to bacterial inflammation [53], or the aggregation of *Dictyostelium discoideum* [54–57]. Effective simulation of biological phenomena at the level of test systems in *in vitro* experiments and the construction of mathematical models is a fundamental method in modern biophysics.

Recent progress in self-organization research in physical, chemical, and biological systems is first and foremost due to the development of an autowave theory including mechanisms of the generation, propagation, and interaction of nonlinear waves in extended active media with diffusion, the so-called active (excitable) media. Such media are exemplified by chains of van der Pol generators, nerve fibers, extended chemical systems with autocatalysis, etc. [6, 8, 58–63]. One common property of the above media is their ability to produce and transmit autowaves, i.e., self-sustained strongly nonlinear medium change waves, whose shape and velocity in an established motion regime are independent of boundary conditions and are totally determined by parameters characterizing a given medium. Autowaves are extended analogs of auto-oscillations in lumped systems. Disturbance of the normal autowave propagation and interaction regimes leads to disorganization and chaos in systems controlled by autowave processes.

All the well-known properties of autowaves have recently been obtained in studies of reaction–diffusion systems. What additional changes are introduced into wave properties of excitable systems by cross-diffusion? Experimental and theoretical studies of the 1980s and 1990s demonstrated that bacterial population waves have much in common with excitation waves propagating in biological systems; they provide an example of autowave processes [2, 23, 64–67]. It was emphasized in the same works that bacterial waves constitute a specific class of autowaves due to their unique properties lacking in ‘classical’ autowaves. Quite unexpected results have been obtained in studies carried out over the last four years [68–73]. It was shown that excitable systems with cross-diffusion exhibit new wave properties that make them substantially different from excitation waves in systems of the reaction–diffusion type. These data allowed categorizing waves in cross-diffusion systems into a special class of nonlinear waves.

This review analyzes results of wave studies in excitable systems with cross-diffusing components.

Section 2 focuses on bacterial population waves propagating due to chemotaxis and considers wave properties in systems with nonlinear cross-diffusion. It presents the results of experimental studies and mathematical models of the formation, propagation, and interaction of bacterial waves and describes conditions for the development of a soliton-like interaction regime.

Sections 3 and 4 deal with taxis wave properties in reaction–diffusion and reaction–taxis systems investigated in a predator–prey model with positive and negative taxes.

The wave propagation mechanism operating in such systems is described. It is shown that the dependence of the taxis wave propagation velocity on the diffusion coefficient is substantially different from the analogous dependence for waves in reaction–diffusion systems. A large region of the parameter space is occupied by the quasi-soliton interaction of taxis waves.

Section 5 discusses a formerly unknown wave phenomenon, half-soliton interaction, studied in one and two-dimensional media.

It is shown in Section 6 that waves in linear cross-diffusion systems are characterized by a quasi-soliton interaction regime. The relation between evolution of wave shape and various wave interaction regimes is discussed.

2. Nonlinear cross-diffusion. Taxis waves

2.1 Taxis in population systems

Nonlinear cross-diffusion systems are exemplified first and foremost by systems with taxis. Waves generated in such systems are called taxis waves. Living organisms can choose a direction of motion due to their ability to respond to environmental changes [22, 74, 75]. This reaction to external stimuli for the choice of the optimal environmental conditions is referred to as a taxis. The directed motion of an organism towards more favorable conditions along the attractant (e.g., nutrient) gradient is a positive taxis, that away from unfavorable factors (e.g., repellents) is a negative taxis [76–78].

In many cases, migration of animals is a response to the diversified environment leading to a temporary concentration of birds in flocks, fish in shoals, flies in swarms, etc. For example, congregation in large groups is one of the principal forms of interactions between individuals ensuring better protection, feeding (searching), and adaptation; it is associated with the ability of individuals to make movements whose intensity and direction are dictated by the nonuniform spatial distribution of a given stimulus [79–82]. The stimulus may be either an environmental factor (temperature, salinity, illumination, food, sound, etc.) or population density.

References [79–82] describe the behavior of animals in space based on the assumption that acceleration of the motion of migrants at each point of space is proportional to the density distribution gradient of a given stimulus. This hypothesis is confirmed by observations of natural populations, e.g., gregarious fish; the probability of a change in the direction of motion (speed variation) depends on the difference between real and preferable temperature [83]. Analysis of the motion of phytophagous insects also suggests that they change the velocity of motion depending on the quality of and closeness to food accumulation [84]. Papers [79–82] propose a mathematical model describing the aggregation of individuals brought together by an autotaxis, i.e., orientation by population density gradient; the model is based on kinematic characteristics of animal motion reported in [85, 86]. Analytic studies of this model [79–82] supplemented by numerical calculations in one- and two-dimensional media suggest formation of a stable stationary concentration of individuals within a certain range of model parameters; that is, the models have a time-independent spatially inhomogeneous solution.

Reference [87] analyzes the wave regimes of conceptual population dynamics described by polynomial reaction–

diffusion–taxis and reaction–cross-diffusion–autotaxis models with an increasing degree of the reaction and taxis (autotaxis) functions. On the one hand, the existence of a ‘proper’ nonlinear taxis may change the speed and the shape of wave fronts and lead to the appearance of various ‘robust’ spatially inhomogeneous wave regimes, including those with a very large density fluctuation amplitude. On the other hand, a taxis may have a stabilizing effect on the spatial distribution dynamics of a system. It is emphasized in the same work that a variety of possible wave regimes may occur at parameter values corresponding to the critical points of a model. In another work [88], the authors examined the role of a taxis in the population dynamics of forest insects [88].

Today, the main experimental and theoretical data on the role of taxis and self-organization processes in population systems come from the studies of bacterial population waves, the growth and development of microbial colonies [22, 23, 65–67, 89–99]. Bacterial populations prove to be convenient subjects for simulation-based analysis of one of the main problems in mathematical biophysics of ecological communities, i.e., investigations into the stability of a regime of ecosystem functioning. Characteristic features of microbial populations, such as multiplicity, rapid generation turnover, controllable growth, and a variety of structural self-organization modalities allow applying the results of their experimental and theoretical studies in the most unusual areas. For example, Ron and collaborators [100] consider certain structural forms of the development of a bacterial colony as possible models of tumor growth.

The chaotic motion of bacteria is known to lead, under certain conditions, to their nonuniform distribution, i.e., to the formation of spatial structures both changing and unchanging with time (see, e.g., [22, 89–91, 101–104]). Extensive studies of the individual and cooperative behavior of bacteria date back to the 1960s when the works of Adler were published [74, 75]. For the past four decades, various aspects of chemotactic mobility have been investigated in much detail (especially in models of population organization in *E. coli* and *Salmonella spp.*) (see reviews [22, 23, 105–107]). The following features of bacterial motility and chemotaxis deserve to be distinguished. Many bacteria have extracellular spiral filiform organelles known as flagella [108–110]. At the base of each flagellum, there is a motor that powers its clockwise or counterclockwise rotation. Individual flagella rotating counterclockwise make up a compact bundle that thrusts the cell forward. Periodically, these smooth/free runs are briefly reversed by jerky chaotic movements reminiscent of vibration and tumbling. They are caused by the untwisting of the bundle as its constituent microfilaments change the direction of rotation [108–111]. Each tumbling episode is followed by reorientation of the cell motion. The direction of an individual cell motion in the absence of a chemotactic gradient is therefore random. Environmental factors attracting bacteria are termed attractants, those having the opposite effect are repellents [74, 75, 108–112]. The free run time in an isotropic medium is $\sim 1-3$ s and a tumbling episode lasts ~ 1.1 s. When a bacterium swims through an attractant gradient, tumbling is partly suppressed; its frequency increases in a repellent gradient.

The molecular mechanism controlling the direction of flagellar rotation is rather complicated [77, 78, 107, 108–114]. A chemoreception model for bacteria in attractant and repellent gradients has been proposed. A variety of receptors are known to interact with attractants or repellents. Most of

them are highly specific and bind to only one or two chemical compounds. The cell analyzes time-dependent environmental conditions for the choice of the optimal behavioral strategy by comparing the degree of receptor occupation and the level of methylation of the part of the receptor submerged in cytoplasm. Occupation of the receptor reflects current environmental conditions and the degree of methylation reflects conditions in the ‘recent past,’ that is, approximately 3 s ago as shown in experiment.

Bacterial attractants and repellents are not only chemical compounds but also physical factors, such as temperature [105, 115], light [116, 117], electric and magnetic fields [118–121], or gravitation [122]. For example, an intense blue light induces continuous tumbling in *E. coli*, while alternating electric fields may stimulate motility in these bacteria and simultaneously inhibit their chemotactic responsiveness.

For a long time, chemotaxis with respect to environmental factors has been regarded as the main cause underlying the mobility of individual bacteria. On the other hand, bacterial cells can by themselves affect this process. For example, *E. coli* and *S. typhimurium* placed under unfavorable conditions release two amino acid attractants, aspartate and glutamate [90, 91, 96, 123]. These cells become mobile sources of attractants and begin to interact with other cells, thus coordinating chemotactic motion. This interaction leads to a variety of nontrivial collective phenomena, e.g., the formation of compact multicellular clusters, mobile rings, and a number of stationary structures of different shape.

Recent studies by Ben-Jacob [102–104] revealed general principles of growth and development of bacterial colonies in terms formerly applied to intellectual systems. In this approach, Ben-Jacob considers bacterial populations as multilevel structured systems with a complicated multicellular hierarchy that are in many respects analogous to social systems composed of individuals having intellect. It is shown that bacteria have numerous means of information exchange for the maintenance of cooperative behavior under unfavorable environmental changes, including a wide range of chemical signal mechanisms, collective gene activation and inactivation, and even exchange of genetic information.

2.2 Bacterial population waves

In the mid-1960s, Adler and collaborators demonstrated that bacteria inoculated in a nutrient medium may generate propagating population waves [74, 75]. Substrate consumption by bacteria leads to a substrate-attractant gradient, and their chaotic movements acquire a component directed along the gradient. Moreover, bacteria continue to multiply. The chemotactic response to the substrate-attractant gradient results in the formation and propagation of taxis rings or bacterial population waves. Taxis rings preserve their clear-cut shape in the course of bacterial motion and propagate with an approximately constant speed depending on the medium (agar) viscosity and strain motility. Constant characteristics are due to continuous reproduction of the local attractant gradient by bacteria as they move from place to place. This wave actually visualizes the boundary between the region of lowered attractant concentration and that where it remains elevated. If the medium contains two attractants consumed by bacteria, two bacterial population waves may form due to depletion of one substrate and subsequent switching of the bacteria to the other, previously disregarded substrate.

Interaction between bacterial waves may cause formation of static spatial structures [22, 66, 89]. The type of structure depends on the wave interaction regime [23, 67]. The present section is focused on two of them (soliton-like and nonsoliton regimes). The former is characterized by penetration of population waves through one another without an apparent delay, the latter by the cessation of colliding waves.

Nonsoliton interaction regime. Figure 1 presents an example of the nonsoliton interaction (the waves stop after collision). Bacteria are initially seeded at four different sites in a slightly agarized nutrient medium in a Petri dish. The sites where bacteria multiply serve as sources of bacterial population waves. We consider the formation of a static cruciform structure from the interaction between bacterial waves moving out from the four inoculation points [66]. These centers give rise to the first ring-shaped chemotaxis waves some 3–4 h after inoculation; the main product consumed by

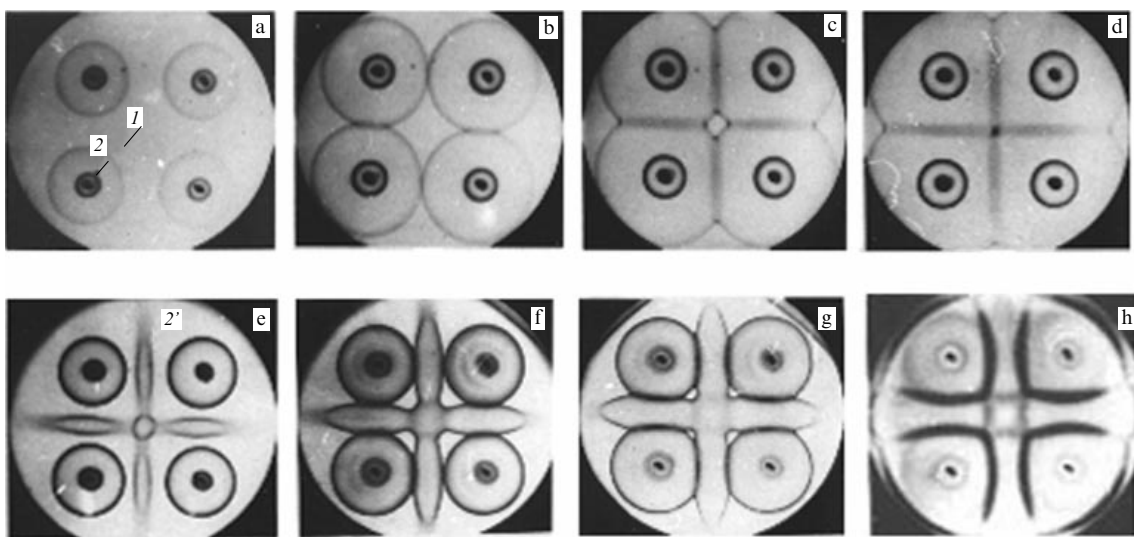


Figure 1. Formation of a cross-like structure in a Petri dish $\varnothing 9$ cm during the interaction of bacterial waves propagating from four sites of *E. coli* J621 inoculation into a nutrient medium [66, 67]. (a) chemotactic rings drawing together ($t = 0$); (b) collision of the first chemotactic rings ($t = 15$ min); (c, d) formation of the collision line ($t = 30$ min, 55 min); (e) ‘reflection’ — formation of waves $2'$ from the collision lines ($t = 85$ min); (f) collision of waves 2 and $2'$ ($t = 140$ min); (g, h) formation of a cruciform structure.

Table 1. Amino acid composition of the nutrient medium (10^{-3} mol) before (control) and after passage of taxis waves of *E. coli J621*.

Medium	Control	1	2	2'
Alanine	1.4	1.4	1.5	1.5
Arginine	2.0	2.1	2.1	2.1
Aspartate	0.3	0.2	0.04	0.03
Glutamate	0.7	0.7	0.6	0.6
Histidine	0.5	0.5	0.5	0.5
Isoleucine	0.4	0.5	0.5	0.5
Leucine	1.5	1.5	1.4	1.3
Lysine	0.8	0.8	0.8	0.8
Methionine	0.2	0.2	0.2	0.2
Phenylalanine	0.9	0.9	0.9	0.9
Praline	0.00	0.00	0.00	0.00
Serine	0.5	0.08	0.03	0.04
Threonine	0.3	0.3	0.2	0.2
Tyrosine	0.9	1.0	1.0	1.0
Valine	1.0	1.0	1.0	1.0

Note: Bold type is used to distinguish components of the medium consumed by bacteria after passage of the first wave (serine) and waves 2 and 2' (aspartate) [66]. Measurements were made with Analaser T339 (Microtechna, Prague)

bacteria from these rings is the serine of the nutrient medium (Table 1). The second ring of chemotaxis waves is formed after a short delay (Fig. 1a). Bacteria of the second wave largely consume aspartate (Table 1). Collision of the first chemotactic rings (Fig. 1b) gives rise to a thin line (Fig. 1b–d) where the waves are stopped by the depletion of the serine gradient.

The rings that stopped upon collision could be expected to undergo diffuse smearing. But this does not occur and bacteria produce waves again. The collision line of the first chemotactic rings gives rise to waves 2' (Fig. 1e) after time τ . As shown in [66], propagation of bacterial waves 2 and 2' is supported by the consumption of identical components of the substrate. Experiments with different nutrient media and microbial strains indicate that after the collision, bacteria from front 1 'switch over' to the attractant along whose gradient wave 2 propagates (in our case, aspartate) (see Table 1). Therefore, the collision of waves 2 and 2' gives rise to the formation of the respective lines (Figs 1g–h).

It was proposed in [65, 66] to regard bacterial population waves 1 and 2 (2') as autowaves of different 'modality.' Unlike autowaves in the previous physical, chemical, and biological studies, bacterial waves of different modality may undergo interconversion due to the ability of bacteria to switch over to an alternative substrate.

What are the factors determining the time τ for which colliding bacterial waves transform into waves 2' moving out from the collision line? It turns out that τ has the least value during the interaction of bacterial waves that propagate in an established regime [99]. Propagation of a bacterial wave is accompanied by an increase in the front density to a constant level in the stationary regime due to division of bacterial cells. When interaction involves chemotaxis waves originating at the inoculation points located close to each other, colliding fronts have low bacterial density; accordingly, the amount of the first substrate-attractant remains rather high and switching over to the second one takes more time [99].

Mathematical model of the formation and propagation of bacterial waves in a multi-component nutrient medium. A mathematical model of chemotaxis wave propagation was

proposed by Keller and Segel in 1971 [124]. We consider a modified Keller–Segel model for the formation and propagation of bacterial waves in a multi-component medium [67]:

$$\frac{\partial b_i}{\partial t} = k_i g(S_i) b_i + \nabla \cdot (\mu(S_i) \nabla b_i) - h_i \nabla \cdot (b_i \chi(S_i) \nabla S_i) + R_i(b, S), \tag{2}$$

$$\frac{\partial S_i}{\partial t} = -p_i g(S_i) b_i + D_S \nabla^2 S_i, \quad i = 1, 2, \dots, m,$$

$$\mu(S_i) = \begin{cases} \mu_0 = D_b, & \text{if } S_i \geq S_{00}, \\ \mu_0 \left(\frac{S_i}{S_{00}} \right)^n, & \text{if } S_i < S_{00}, \end{cases} \tag{2a}$$

$$R_i(b, S) = r_{i-1} b_{i-1} - r_i b_i, \tag{2b}$$

$$r_i = \begin{cases} 0, & \text{if } S_i > S_{hi}, \\ \alpha (0 < \alpha < 1), & \text{if } S_i < S_{hi}, \end{cases}$$

$$\chi(S_i) = \frac{S_i}{(S_i + S_k)^2}, \quad g(S_i) = \frac{S_i}{S_i + S_r}, \tag{2c}$$

where $b_i(x, y, t)$ is the concentration of bacteria consuming the substrate component $S_i(x, y, t)$, S_{hi} is the threshold value of substrate S_i , D_b and D_S are the diffusion coefficients of the bacteria and substrate, respectively, $\chi(S_i)$ is the chemotactic response function, $g(S_i)$ is the specific bacterial growth rate, h is the taxis coefficient, and $S_k, S_r, S_{hi}, S_{00}, k_i, p_i, r_i$, and α are constants. The function $R_i(b, S)$ describes the transformation of bacteria b_{i-1} consuming the substrate S_{i-1} to a subpopulation b_i consuming the substrate S_i . The classical Keller–Segel model is recovered at $m = 1$ and $\alpha = 0$, i.e., for a one-component medium and, accordingly, without bacteria switching over to the consumption of other substrate-attractants.¹

Figure 2 presents the result of numerical simulation of the formation of a cross-shaped structure during the interaction between bacterial waves moving out from four inoculation centers. Figure 2b details the propagation and interaction dynamics of waves produced only by b_2 -type bacteria (waves 2 and 2') both in the four inoculation centers and upon collision of waves of bacteria b_1 and their switching to the substrate S_2 after the interval of $\tau \approx 25$ arbitrary time units.

It follows from experiment (see Fig. 1) and simulation (Fig. 2) that this interaction regime is a nonsoliton one because population waves 1 stop upon collision and do not pass through one another. Wave passage/reflection is associated with switching over to the consumption of another substrate. This switching takes some time to be completed.

2.3 Restoration of bacterial population waves during isolation of the inoculation center

The dependence of bacterial wave formation on initial conditions was studied both by mathematical modeling and in experiments on perturbation of propagation of two successive chemotaxis rings of *E. coli* with isolation of a region around the inoculation point that serves as a source of such waves. It was shown that such excitation does not interfere with the generation of the second chemotaxis wave [93].

¹ See review [22] for more details pertaining to the Keller–Segel model [2].

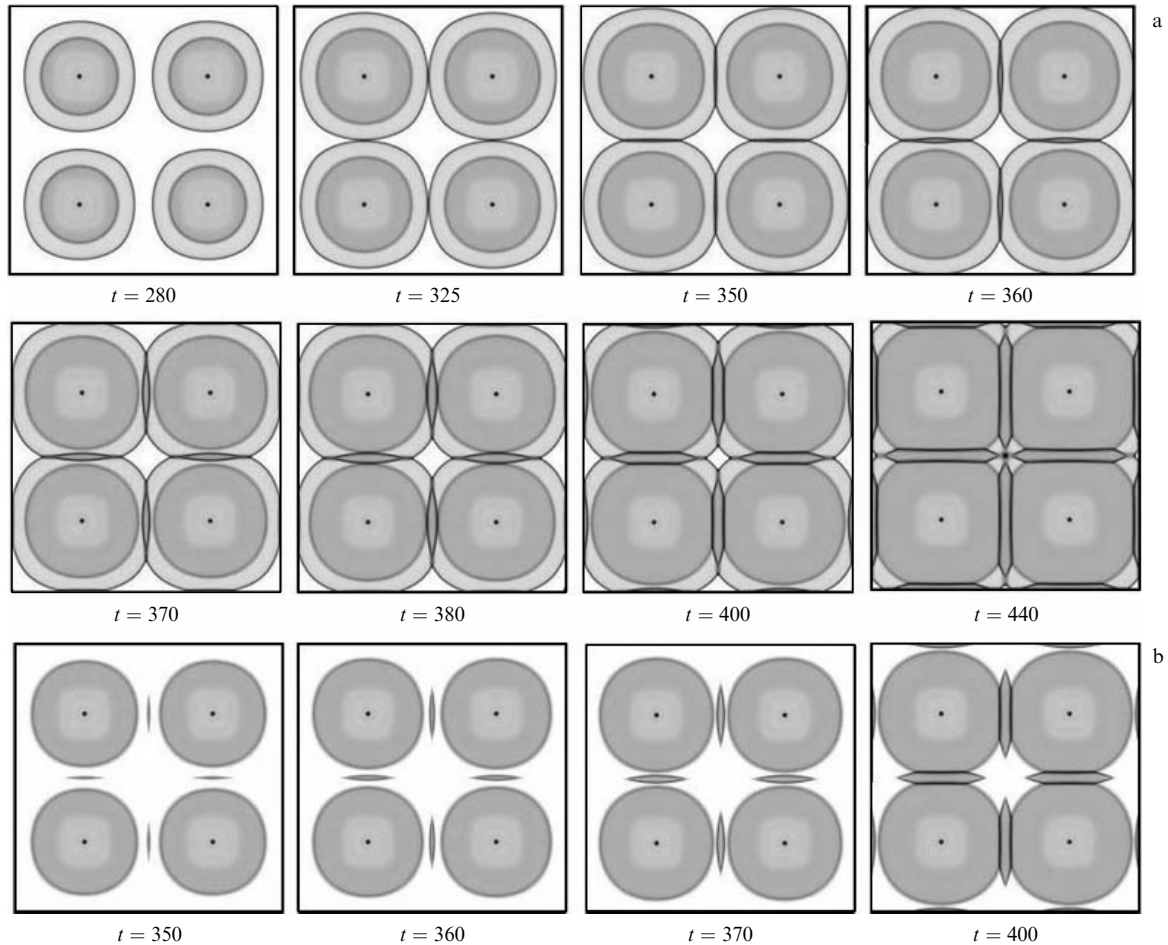


Figure 2. Formation of a cross-shaped structure in a numerical experiment in mathematical model (2) of a two-component medium ($m = 2$) of size $L_x \times L_y = 210 \times 210$ [99]. (a) propagation and interaction waves of bacteria $b = b_1 + b_2$; (b) formation, propagation, and interaction dynamics of population waves (2 and 2') of bacteria b_2 . Parameters of the model: $h_1 = 0.4$, $h_2 = 0.2$, $S_k = 5 \times 10^{-3}$, $S_c = 0.55$, $S_{b1} = 10^{-5}$, $S_0 = 0.05$, $\alpha = 0.1$, $S_{00} = 0$, $b_0 = 0.8$, $D_b = 0$, $D_S = 0$, $k_1 = k_2 = 1$, $p_1 = p_2 = 0.4$. Coordinates of inoculation centers (x_c, y_c) : (55, 55), (155, 55), (55, 155), (155, 155).

Mathematical simulation was based on model (2) in a two-dimensional medium in the two-component case ($m = 2$) with the initial conditions $S_1(x, y, 0) = S_2(x, y, 0) = S_0$, $x_c = L_x/2$, $y_c = L_y/2$, where (x_c, y_c) are coordinates of the center of the inoculation region of bacteria (b_0) with the radius R_0 . Results of numerical experiments are shown in Fig. 3a. After the formation of two waves propagating along the substrate attractants S_1 and S_2 (Fig. 3, $t = 60$) at the instant $t^* = 70$, the vicinity of the inoculation center with the radius $R = 30$ was cut out so as to isolate the second wave:

$$S_1(x, y, t^*) = S_2(x, y, t^*) = 0,$$

$$b_1(x, y, t^*) = b_2(x, y, t^*) = 0,$$

$$\text{if } \sqrt{(x - x_c)^2 + (y - y_c)^2} < R.$$

As the wave propagated along the substrate S_1 , bacteria falling behind the first wave front gave rise to the second wave consuming the substrate S_2 .

What is the mechanism of this process? It follows from mathematical model (2) that the switching of bacteria from the consumption of one substrate to another occurs only if the concentration of the former decreases to a threshold level S_{b1} . When the propagation velocity and bacterial density of the

first wave are constant, the concentration of the substrate $S_1(x, y)$ at each point decreases to S_{b1} at equal intervals after the passage of the wave front. Therefore, when the inoculation center and its close vicinity to the second wave are isolated, bacteria within a circle of radius R are the first to switch over to the consumption of the second substrate-attractant. This results in the propagation of bacteria that fell behind the first chemotactic ring and switch over to the substrate S_2 . The presence of a substrate-attractant concentration gradient is necessary for the existence of a chemotaxis wave. Evidently, the substrate S_2 gradient created within a circle of radius R provides the condition for directed bacterial movements. The spatial density of bacteria propagating in a given direction along the gradient of S_2 is enhanced by bacteria that consecutively switch over to the consumption of S_2 at $r > R$. These factors create prerequisites for the formation of the second chemotactic ring.

The results of numerical simulation were confirmed in experiments on the formation of bacterial population waves. In these experiments, *E. coli J621* were inoculated into the center of a Petri dish 9 cm in diameter containing a slightly agarized ~ 2 mm thick nutrient medium (peptone 1.5%, Difco agar 0.27%, NaCl 0.5%). The dish was previously filled with a ~ 2 mm thick strongly agarized substrate of 2% Difco agar and 0.5% NaCl for the reliable isolation of the

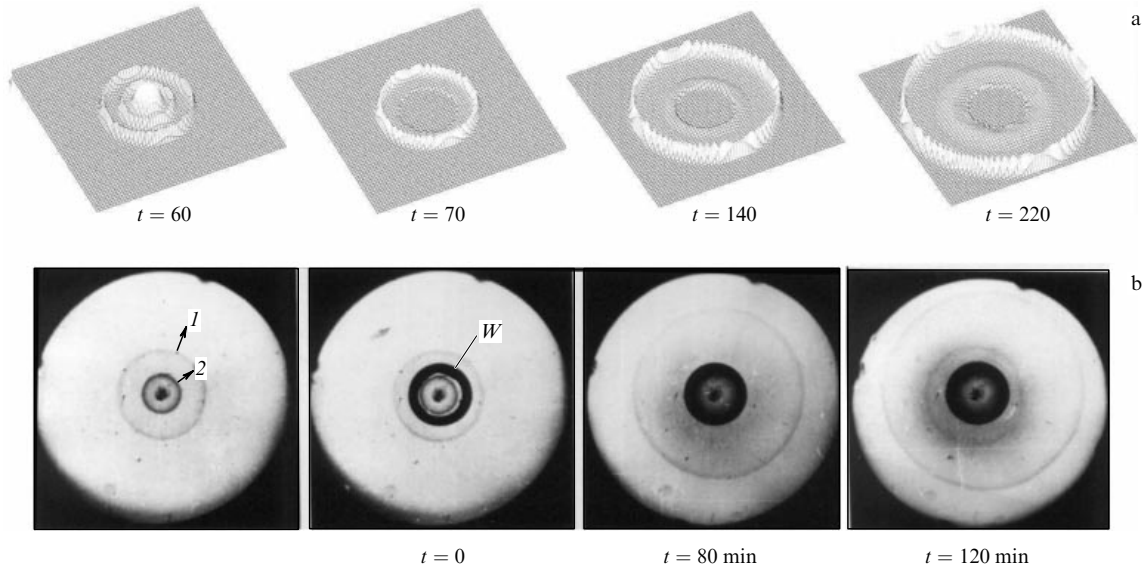


Figure 3. Formation and propagation of the second bacterial wave during isolation of the inoculation center [93]. (a) Results of numerical experiments with mathematical model (2). Two-component medium ($m = 2$) of size $L_x \times L_y = 250 \times 250$. Parameters of the model: $h_1 = 4, h_2 = 2, S_r = 0.7, S_k = 5 \times 10^{-3}, S_{h1} = 5 \times 10^{-4}, S_0 = 0.05, \alpha = 1, S_{00} = 0, b_0 = 1, D_b = 0, D_S = 0, k_1 = k_2 = 1, p_1 = p_2 = 0.4, R = 30$. (b) Population waves of *E. coli J621*: propagation of the first (I) and the second (2) chemotaxis rings from the inoculation center, isolation of the second ring with a cylindrical membrane W ($t = 0$); formation of the second chemotaxis ring outside the membrane ($t = 80$ min, $t = 120$ min).

inoculation center. The center was isolated by an impenetrable cylindrical membrane after formation of the second bacterial wave such that the entire second front was enclosed by the membrane.

The results of these experiments are shown in Fig. 3b. It can be seen that isolation of the inoculation center and the second wave (Fig. 3b, $t = 0$) does not prevent formation of a new wave at a distance from the enclosed region by residual bacteria of the first chemotaxis ring (Fig. 3b, $t = 80$ min, $t = 120$ min). The appearance and movement of the second front are due to the adaptation of bacteria to environmental changes rather than to the initial conditions.

2.4 Soliton-like regime of the interaction between bacterial waves

Mathematical simulation and experiment in [67] demonstrated for the first time that the studied bacterial population system also exhibited a soliton-like regime of chemotactic ring interactions. As bacterial waves collided at a speed slightly higher than a certain critical value, they penetrated through/reflected from one another without an apparent delay. Figure 4a shows the soliton-like interaction dynamics of bacterial waves in numerical experiments with model (2) and Fig. 4b shows the population wave interaction dynamics of *E. coli* in a slightly agarized nutrient medium.

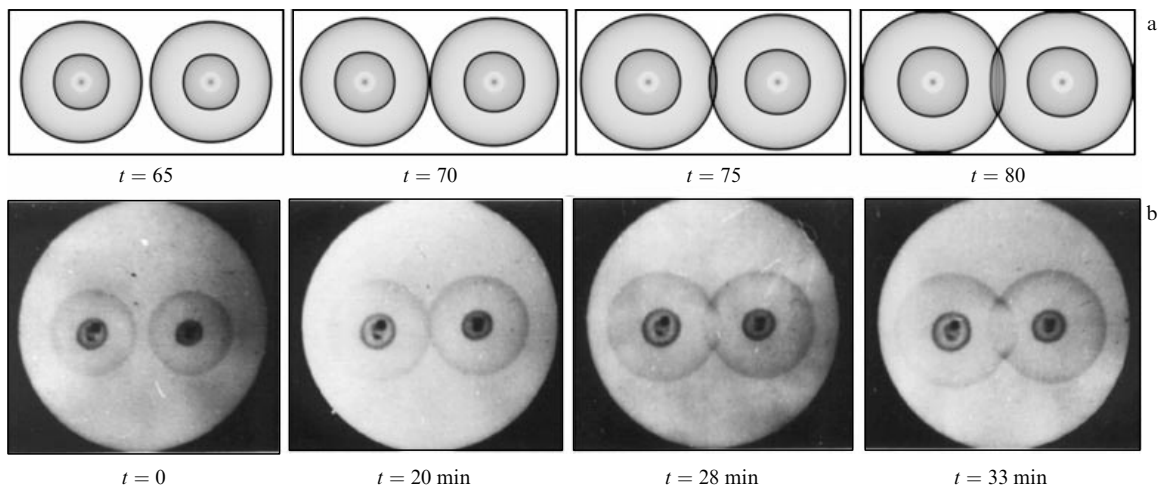


Figure 4. Soliton-like regime of bacterial population wave interaction. (a) Numerical experiments with mathematical model (2) for a two-component medium ($m = 2$) of size $L_x \times L_y = 210 \times 110$ [99]. Parameters of the model: $h_1 = 6, h_2 = 3$, the remaining ones (*E. coli J621*) are as in Fig. 2. Coordinates of the inoculation centers (x_c, y_c) : (55, 55), (155, 55). (b) Interaction between bacterial waves (*E. coli J621*) originating from two inoculation centers in a weakly agarized nutrient medium (1% peptone, 0.5% NaCl, 0.22% agar Typ USA, $\sim 1-2$ -mm-thick layer, petri dish ($\varnothing 9$ cm), 37°C). Colliding waves ($t = 20$ min) pass through/reflect from one another without an appreciable delay ($t = 28$ min, $t = 33$ min) [67].

What is the mechanism of this interaction? It is known that the strength of a chemotactic response largely depends on the ratio dS/S (where S is the substrate-attractant concentration) [125]. This means that a high consumption rate of the substrate, even at its low concentration, may create a rather marked attractant gradient. At the onset of front contacts, the bacterial concentration at the collision point increases, and the bacteria located at this site create a new concentration gradient of the first substrate remaining after the wave passage. If a certain amount of the first substrate remains at the bacterial front and behind it, the newly created gradient is sufficient to maintain directed movements of bacteria without their switching to the consumption of the second substrate. The wave then propagates along the first attractant as far as the medium region, where it is depleted due to the consumption of the substrate by a small number of bacteria that always fell behind the first chemotaxis ring during its expansion.

The bacterial-wave propagation speed V depends on the agar concentration in the nutrient medium. It was shown by varying the agar concentration in the nutrient medium [67] that the soliton-like interaction regime between bacterial waves (*E. coli J621*) developed at a relatively high expansion rate of chemotactic rings; specifically, the soliton-like regime at $V > 9 \text{ mm h}^{-1}$, the nonsoliton regime at $4.5 < V < 9 \text{ mm h}^{-1}$, and a collisionless interaction regime at $V < 4.5 \text{ mm h}^{-1}$ [92]. In numerical experiments with model (2), the shift of the nonsoliton interaction regime to the soliton-like one also occurred with an increase in the wave propagation speed resulting from a change in the taxis coefficient h .

3. Main properties of population taxis waves

Mathematical model. We consider population taxis waves using a reaction–diffusion mathematical model of the predator–prey type with directed motion of predators toward the prey and evasion behavior of the prey [9]. Such problems were studied with cellular automata models including predators pursuing prey and prey escaping predators [126–128]. Properties of nonlinear waves in a one-dimensional predator–prey mathematical model were first comprehensively studied in [68, 69]. A new type of wave propagation in reaction–diffusion–taxis and reaction–taxis systems underlain by a taxis-dependent mechanism was demonstrated in [68, 69], where quite unexpected results were obtained.

We consider a one-dimensional reaction–diffusion–taxis system describing a predator–prey model whose spatial evolution is governed by three processes: diffusion of both variables, a positive taxis of predators up the gradient of prey, and a negative taxis of prey down the gradient of predators:

$$\begin{aligned} \frac{\partial P}{\partial t} &= f(P, Z) + D \frac{\partial^2 P}{\partial x^2} + h_- \frac{\partial}{\partial x} P \frac{\partial Z}{\partial x}, \\ \frac{\partial Z}{\partial t} &= g(P, Z) + D \frac{\partial^2 Z}{\partial x^2} - h_+ \frac{\partial}{\partial x} Z \frac{\partial P}{\partial x}, \end{aligned} \quad (3)$$

where $P(x, t)$ and $Z(x, t)$ are the prey and predator population densities, respectively, the diffusion coefficients of P and Z are assumed to be equal to D , $\partial/\partial x (P(\partial Z/\partial x))$ are taxis terms, $\partial/\partial x (Z(\partial P/\partial x))$ is the coefficient of a negative P taxis down the Z gradient, and h_- is the coefficient of a positive Z taxis up the P gradient. Local kinetic functions $f(P, Z)$ and $g(P, Z)$ were taken as in Refs [129, 130], which reported a

Truscott–Brindley reaction–diffusion model describing the population dynamics of phytoplankton (P) and zooplankton (Z):

$$\begin{aligned} f(P, Z) &= \beta P(1 - P) - \frac{ZP^2}{P^2 + \nu^2}, \\ g(P, Z) &= \frac{\gamma ZP^2}{P^2 + \nu^2} - wZ, \end{aligned} \quad (3a)$$

where β, γ, ν, w are constants.

Such kinetics is known to display ‘excitable’ behavior; in other words, it implies the possibility of propagation of a solitary wave at certain parameters of the reaction–diffusion system ($h_- = h_+ = 0$). Model (3), (3a) has dimensionless variables and parameters.

All numerical experiments in the study of mathematical model (3) of the reaction–diffusion–taxis ($D > 0$, $h_- > 0$ and/or $h_+ > 0$) and reaction–taxis ($D = 0$, $h_- > 0$ and/or $h_+ > 0$) types were performed using the upwind difference scheme proposed in [69]. This scheme, unlike the classical central scheme, allows computation not only at small diffusion coefficients D but also at $D = 0$.

If not specified otherwise, calculations were carried out at the parameter values $\beta = 1$, $\nu = 0.07$, and $w = 0.004$ and two different values of γ :

(a) $\gamma = 0.01$, at which wave propagation occurs through diffusion alone (i.e. at $h_- = h_+ = 0$, $D > 0$);

(b) $\gamma = 0.016$, at which the propagation of a purely diffusion wave is infeasible.

3.1 Waves in a reaction–diffusion–taxis system

($\gamma = 0.01$)

Figure 5 presents profiles of population waves described by the system of equations (3) in the reaction–diffusion case (Fig. 5a) and after the addition of taxis terms (Figs 5b, c, e–g). The taxis terms substantially change the wave profile, with the coefficient h_+ making a much greater contribution than h_- . If $h_- > 0$, the waves retain the same shape as in the purely diffuse case with a long and smooth plateau. At $h_+ > 0$, the wave profile of Z becomes explicitly nonmonotonic, while waves of the variable P have two profiles, ‘one-humped’ and ‘two-humped.’

For a qualitative explanation of the change in the wave shape, we consider the effect of a positive Z taxis up the P gradient for $h_+ > 0$. Prior to wave propagation, the system is stable. A local increase in the P density in an interval $0 < x < x_0$ induces the flow of Z from the vicinity in front of the point x_0 toward the P gradient. As a result, the equilibrium in front of the point x_0 is disturbed by a decrease in the Z density which, in turn, leads to an increase in the P density. A sequence of such events gives rise to a traveling wave. Diffusion is not necessary for the realization of this wave formation mechanism. The same mechanism accounts for oscillations ahead of the taxis wave front (Fig. 5d, h). The amplitude of these oscillations being low, they can be described in the framework of a linearized theory. When the wave propagates with an established speed c , the variables P and Z depend only on the combination $\xi = x - ct$ and satisfy the automodel system

$$\begin{aligned} f(P, Z) + D \frac{d^2 P}{d\xi^2} + h_- \frac{d}{d\xi} P \frac{dZ}{d\xi} + c \frac{dP}{d\xi} &= 0, \\ g(P, Z) + D \frac{d^2 Z}{d\xi^2} - h_+ \frac{d}{d\xi} Z \frac{dP}{d\xi} + c \frac{dZ}{d\xi} &= 0. \end{aligned} \quad (4)$$

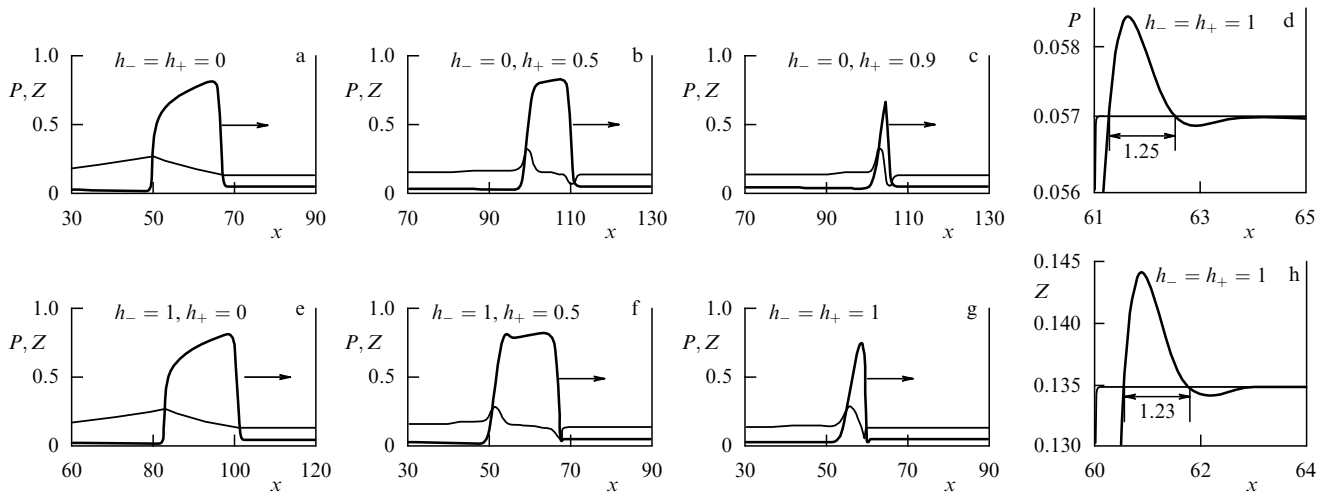


Figure 5. (a–c, e–g) Taxis waves in system (3) (P — thick lines, Z — thin lines) at different coefficients h_+ ($D = 0.04$, $\beta = 1$, $\gamma = 0.01$, $w = 0.004$). (d, h) Pulse forefront oscillations (theoretical half-length value is 1.256), horizontal lines correspond to the steady state (P_0, Z_0) [68, 69].

In Fig. 5g, the wave speed is $c = 0.3535$, and stationary values of P_0 and Z_0 are 0.05703 and 0.13480, respectively. Simple calculations using these parameters give the solution in the form

$$(P, Z)(\xi) \approx (P_0, Z_0) + \text{Re}[(P_1, Z_1) \exp(-\lambda \xi)],$$

$$|P_1, Z_1| \ll |P_0, Z_0|, \quad \lambda \approx 1.9925 + 2.5014i.$$

It follows that the oscillation half-length along the coordinate ξ is $\pi/\text{Im} \lambda_{1,2} \approx 1.256$, in good agreement with the observed wave profiles (Fig. 5d, h). In other words, these oscillations are not a numerical artifact [68].

Taxis waves have an important property of retaining their shape, amplitude, and velocity; that is, once established after a transitional period, these characteristics are independent of the initial conditions [68, 69]. In this respect, they resemble autowaves and differ from waves in conservative systems.

The main differences in the mechanisms of wave propagation in reaction–diffusion and reaction–taxis systems may be characterized as follows. The density of predators in the forefront of a reaction–diffusion wave changes slowly. The wave front usually spreads through diffusion and local nonlinear dynamics of the prey. The density of predators gradually increases between the forward and rear fronts as they consume the prey. It becomes especially high at the back front, where the prey concentration decreases substantially. Here, as at the forefront, the diffusion of P and Z has a marked effect. Quite a different sequence of events occurs in the reaction–taxis system. As mentioned above, the forefront of P attracts Z , which results in the movement of Z towards the P front. A second mechanism then operates whereby the forefront of P spreads due to the negative taxis of prey down the gradient of predators. The same shifting mechanisms for P and Z determine the shape of the rear front and account for the taxis wave duration (τ) being significantly shorter than that of a diffusion wave [70].

Quasi-soliton interactions of taxis waves. It was shown in [68, 69] that system of equations (3) has a region in the parameter space characterized by a quasi-soliton wave interaction during which the colliding waves penetrate

through (reflect from) one another and undergo reflection from the boundaries. This is the main difference from classical autowaves in excitable media [62]. Figure 6 presents the results of numerical experiments on a segment of length L with impenetrable boundaries ($\partial P/\partial x|_{x=0,L} = 0$ and $\partial Z/\partial x|_{x=0,L} = 0$); two waves were started from either end of the segment; the data obtained are given in the coordinates t and x . Purely diffuse waves annihilate upon collision (Fig. 6a). The introduction of taxis terms leads to two types of interactions: (b) a quasi-soliton interaction during which waves penetrate through one another to be reflected from the boundaries and (c) the splitting of waves after they pass through one another (or were reflected from the boundaries); in this case, rear fronts emit backward waves that collide and annihilate.

Soliton-like interactions occur in certain reaction–diffusion systems with excitable kinetics (autowaves) in both mathematical models [131–138] and experiment [138, 139]. However, such interactions are always confined to a very narrow parameter region at the boundary of the standby and oscillatory regimes of the system [134–137]. Analysis of the transition from the annihilation regime to the soliton-like one upon the collision of two waves is reported in [140–141] based on the FitzHugh–Nagumo reaction–diffusion mathematical model [142, 143].

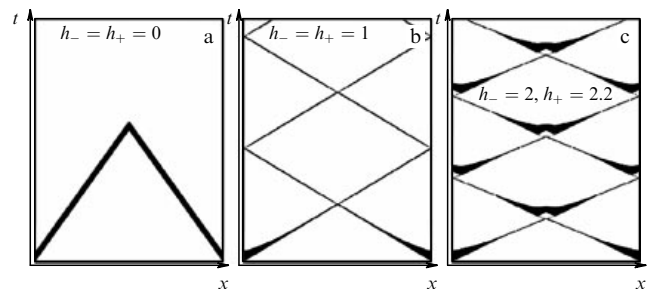


Figure 6. Spatio-temporal dynamics of the propagation and interaction of waves (3) at different taxis coefficients h_{\pm} [69]: (a) wave annihilation; (b) quasi-soliton interaction; (c) quasi-soliton interaction with splitting of waves upon collision. In all cases, $D = 0.04$, $L = 500$, and $t \in [0, 3000]$.

It is shown in [68, 69] that the quasi-soliton regime for excitable systems with cross-diffusion occurs in a large area of the parameter space.

Different taxis wave propagation and interaction regimes are depicted in Fig. 7 for several parameter spaces. The following regimes are characteristic of reaction–diffusion–taxis systems (3), (3a) (Figs 7a–c):

- (1) propagation of waves annihilating upon interaction,
- (2) propagation with splitting,
- (3) quasi-soliton interaction, i.e., penetration of waves through one another, and
- (4) quasi-soliton interaction with splitting.

Another qualitative difference between taxis waves and ‘classical’ autowaves is that they do not immediately annihilate, like autowaves in reaction–diffusion systems, even in the nonsoliton interaction regime (Fig. 8a), but pass through one another and only then decay.

Wave splitting. The phenomenon of taxis wave splitting is observable in both quasi-soliton (black triangles in Fig. 7) and nonsoliton (white triangles, Fig. 7) interaction regimes. Figure 9 illustrates different h_+ -dependent regimes in one-dimensional taxis waves in a medium with impenetrable boundaries. The time interval between successive splittings increases with increasing h_+ (Fig. 9b, c). A split wave propagating backward either decays or undergoes secondary splitting. In the latter case, this process may lead to self-supporting aperiodic or periodic activity.

As shown in [69], splitting is immediately preceded by the oscillatory instability of a propagating wave manifested as the increasing amplitude of P and Z oscillations. Each splitting has only a weak effect on the forefront propagation velocity, and the process itself remains periodic [69].

Similar wave splittings were observed in experiments with the Belousov–Zhabotinskii reaction [144], in numerical

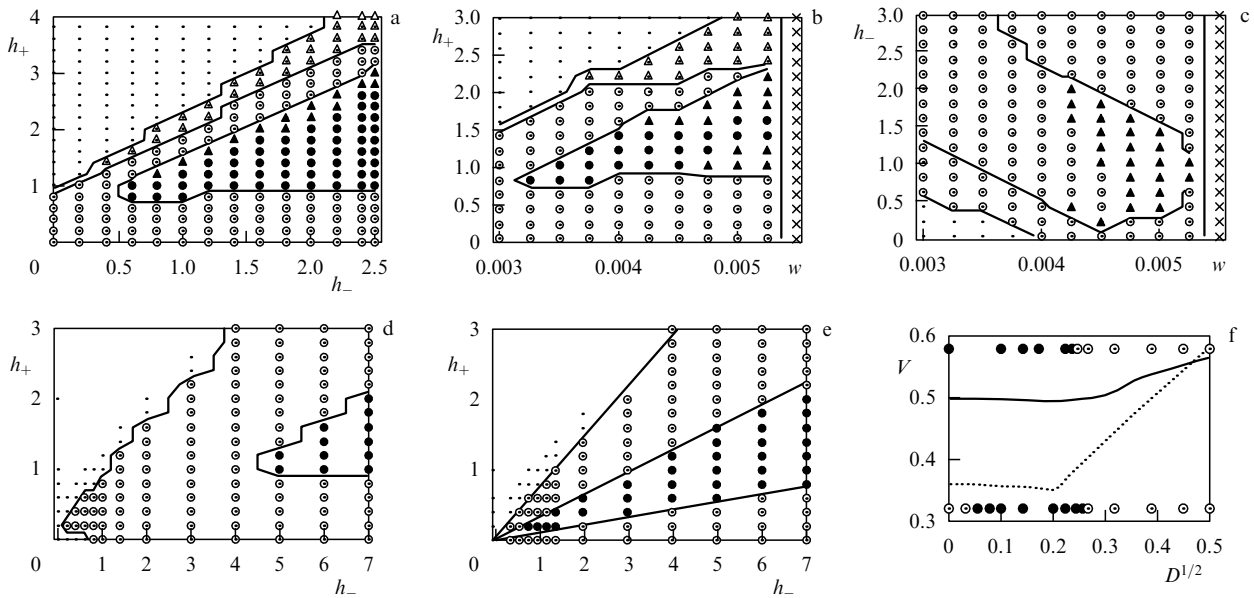


Figure 7. Parameter space corresponding to different taxis wave propagation and interaction regimes [68, 69]: (a) $\gamma = 0.01$, $D = 0.04$, $\beta = 1$, $w = 0.004$; (b) $\gamma = 0.01$, $D = 0.04$, $\beta = 1$, $h_- = 1$; (c) $\gamma = 0.01$, $D = 0.04$, $\beta = 1$, $h_+ = 1$; (d) $\gamma = 0.016$, $D = 0.04$, $\beta = 1$, $w = 0.004$; (e) $\gamma = 0.016$, $D = 0$, $\beta = 1$, $w = 0.004$; (f) taxis wave propagation velocity as a function of $D^{1/2}$. Solid line — $\gamma = 0.016$, $h_- = 5$, $h_+ = 1$, dotted line — $\gamma = 0.01$, $h_- = h_+ = 1$. In reaction–diffusion systems, this dependence is always linear. ● — quasi-soliton interaction, ○ — quasi-soliton interaction with wave splitting, ▲ — persistent pulse propagation with nonsoliton interaction, △ — pulse propagation with splitting, • — unstable propagation, × — oscillation regime.

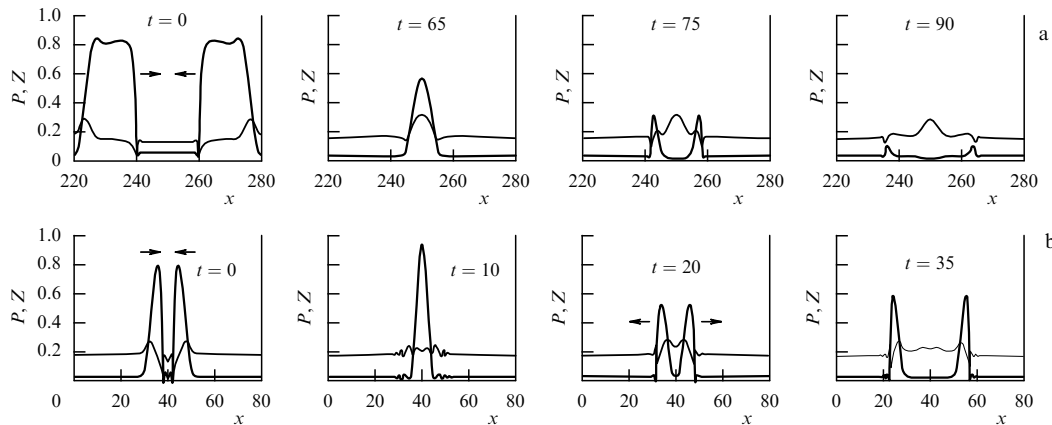


Figure 8. Two taxis wave interaction regimes [68, 69]: (a) nonsoliton ($\gamma = 0.01$, $D = 0.04$, $h_- = 2$, $h_+ = 0.85$) — waves penetrate through one another and only then decay, (b) quasi-soliton ($\gamma = 0.016$ and $D = 0$, $h_- = 5$, $h_+ = 1$) — waves penetrate through one another and their amplitude is gradually restored.

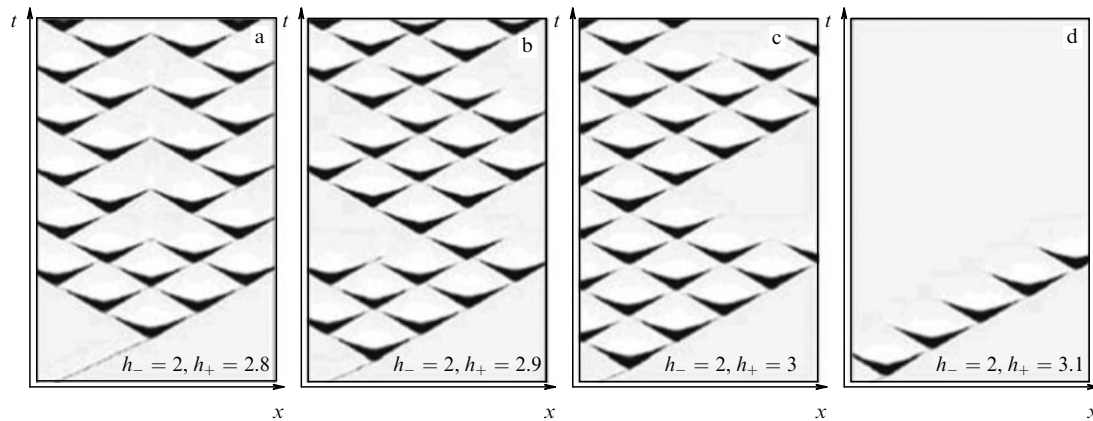


Figure 9. Spatio-temporal dynamics of taxis wave propagation and interaction in the splitting regime [69] ($L = 600, t \in [0, 3000]$).

experiments with the FitzHugh–Nagumo model and a mathematical model of the Belousov–Zhabotinskii reaction [145, 146], and in a three-component reaction–diffusion model describing blood coagulation [147].

Taxis wave propagation velocity. Figure 10a shows the typical h_+ -dependence of the taxis wave propagation speed at different fixed h_- values. Symbols in this figure denote different wave propagation and interaction regimes. The graphs have two branches, parabolic and linear. The linear branch is virtually independent of h_- above a certain h_+ value. It turns out that the transition of the parabolic branch to the linear one with increasing h_+ shows linear correlation with a quantitative change in the wave shape [69]. The parabolic branch corresponds to the ‘two-humped’ shape of $P(x)$ and the linear one to the ‘one-humped’ shape.

3.2 Waves in a reaction–taxis system ($\gamma = 0.016$)

The preceding section was focused on taxis waves in the case where local kinetics allows purely diffuse waves in the system of equations (3), i.e., for $h_- = h_+ = 0, D > 0$. Local kinetic parameters can be changed so as to make such propagation unfeasible. This regime occurs when the parameter γ increases in a mathematical model. It turns out that taxis waves can also propagate in this case.

Figure 7d shows the dependence of taxis wave behavior on h_- and h_+ at fixed $\gamma = 0.016$ and $D = 0.04$. The point

$h_- = h_+ = 0$ is in the region where stationary wave propagation is impossible. The plane h_-, h_+ has regions corresponding to quasi-soliton and nonsoliton wave interactions. No wave splitting is observed in this parameter region, in contrast to the case of local kinetics considered for $\gamma = 0.01$.

We consider a situation where the diffusion coefficient $D = 0$ (Fig. 7e). The h_+ -dependence of the wave propagation speed is illustrated in Fig. 10b. Here, the graph also has two branches, and the transition from the parabolic to linear branch (Fig. 10b) correlates with the transition from a ‘two-humped’ to a ‘one-humped’ wave [69]. This transition is well correlated with the transition from quasi-soliton to nonsoliton wave interaction regimes [69]. As in the previous case, taxis waves do not annihilate in the nonsoliton interaction regime at $\gamma = 0.016$ for $D \geq 0$ but always penetrate through one another prior to decay [69].

3.3 Mechanisms of the quasi-soliton interaction between taxis waves

We consider the quasi-soliton interactions of taxis waves in the case where $\gamma = 0.016$ and $D = 0$ at greater length (Fig. 8b). It was mentioned above that taxis waves in the mathematical predator–prey model are characterized by low density of predators (Z) ahead of the prey wave front (P) because the predator moves along the prey density gradient due to positive taxis. The predator and the prey move in opposite directions. The meeting of two waves of the

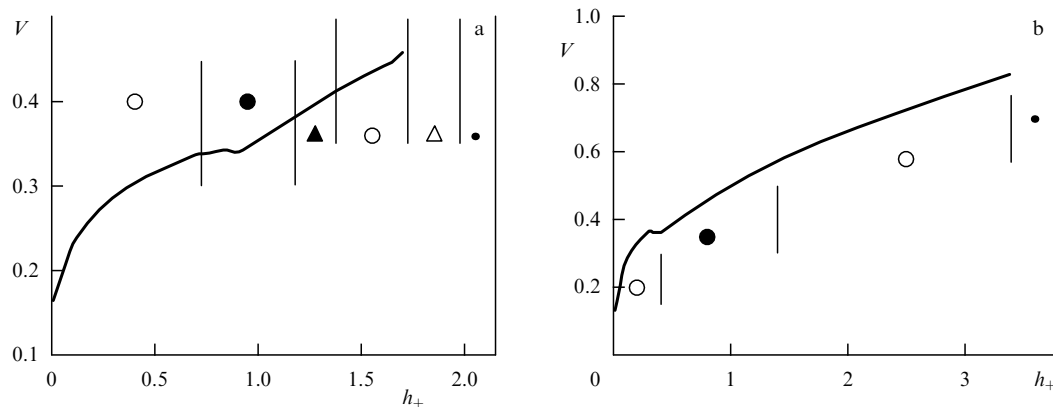


Figure 10. The h_+ dependence of the taxis wave propagation speed V at fixed h_- [69]: (a) $\gamma = 0.01, D = 0.04, h_- = 1$; (b) $\gamma = 0.016, D = 0, h_- = 5$. Vertical lines separate regions corresponding to different interaction regimes (see Fig. 7 for the notation).

prey results in its enhanced concentration (Fig. 8b, $t = 10$). High local concentration of the prey attracts predators, which leave the periphery of the collision zone. A local increase in the number of predators provokes ‘evasion’ of prey (due to a negative taxis down the gradient of predators) from the center of the collision zone towards its boundaries where the predator density has already decreased (Fig. 8b, $t = 20$). The result is the inversion of population gradients and formation of new fronts at the boundaries of the collision zone. In this way, two new (reflected) taxis waves are generated that gradually recover their normal amplitude (Fig. 8b, $t = 35$).

As noted above, certain properties of taxis waves are essentially different from autowave properties. The dependence of the wave propagation speed on the diffusion coefficient D is also different (Fig. 7f). Evidently, the dependence presented in the figure is different from the $\propto D^{1/2}$ law in reaction–diffusion waves. This dependence is disturbed near the transition between annihilating and reflected waves.

To conclude, the observed properties of taxis waves are not mathematical exotics as confirmed by the existence of the soliton-like interaction regime in bacterial populations [67] (Fig. 4b).

4. Taxis waves in two-dimensional media

Mathematical model. We consider a two-dimensional version of mathematical model (3) [70]:

$$\frac{\partial P}{\partial t} = f(P, Z) + D\nabla^2 P + h_- \nabla(P \nabla Z), \quad (5)$$

$$\frac{\partial Z}{\partial t} = g(P, Z) + D\nabla^2 Z - h_+ \nabla(Z \nabla P),$$

where $P(x, y, t)$ and $Z(x, y, t)$ are the respective population densities of prey and predator. The local kinetic functions $f(P, Z)$ and $g(P, Z)$ satisfy system (2a) with the parameters $\beta = 1$, $\nu = 0.07$, $w = 0.004$, and the parameters γ and D are considered in two variants: (A) $\gamma = 0.01$, $D = 0.04$ and (B) $\gamma = 0.016$, $D = 0$. The taxis coefficients h_- and h_+ vary. As known from the one-dimensional case, propagation of a purely diffuse wave without taxis terms ($h_- = h_+ = 0$) is feasible in variant (A), but no such waves are possible in variant (B).

All two-dimensional numerical experiments were made on rectangular or square media $(x, y) \in [0, L_x] \times [0, L_y]$ with impenetrable boundaries:

$$\frac{\partial(P, Z)}{\partial x} \Big|_{x=0, L_x} = \frac{\partial(P, Z)}{\partial y} \Big|_{y=0, L_y} = 0. \quad (6)$$

The numerical experiments were carried out using the explicit Euler scheme with numerical approximation of the taxis term by the explicit upwind difference scheme [69] with spatial and temporal steps $\delta x = \delta y = 0.5$ and $\delta t = 0.005$. In figures showing pictures with a regular time interval, this interval is denoted by Δt .

4.1 Spiral waves

Rotating spiral waves are a special type of elementary excitations in two-dimensional active media described by reaction–diffusion systems [148–152]. The spiral wave is the fastest of the autonomous autowave sources; its frequency

is higher than in the leading (circular) center. Spiral waves are long-known and extensively studied processes in two-dimensional reaction–diffusion systems observed in a variety of experimental conditions. Accordingly, there is a variety of mathematical models describing such systems including predator–prey models [153]. In what follows, we consider results of investigations into the properties of spiral waves in excitable media of the reaction–diffusion–taxis and reaction–taxis types [70].

Very low taxis can destabilize spirals. Figure 11a depicts a typical stable spiral-wave solution observed in the purely reaction–diffusion model (5). Results of the study of taxis wave properties in the one-dimensional case [68, 69] suggest a qualitatively new behavior of spiral waves, when taxis terms are large enough in comparison with the diffusion coefficient D (in our case, $D = 0.04$). This value corresponds to fluxes comparable in terms of diffusion and taxis. Comparison of the fluxes allows the relative contribution of taxis and diffusion terms to be reasonably evaluated. It must be remembered that the coefficients of nonlinear terms (h_{\pm}) and D have different dimensions.

Figure 11b shows a spiral wave in a reaction–diffusion–taxis system at taxis coefficients significantly smaller than those at which reflection from the boundaries occurs.

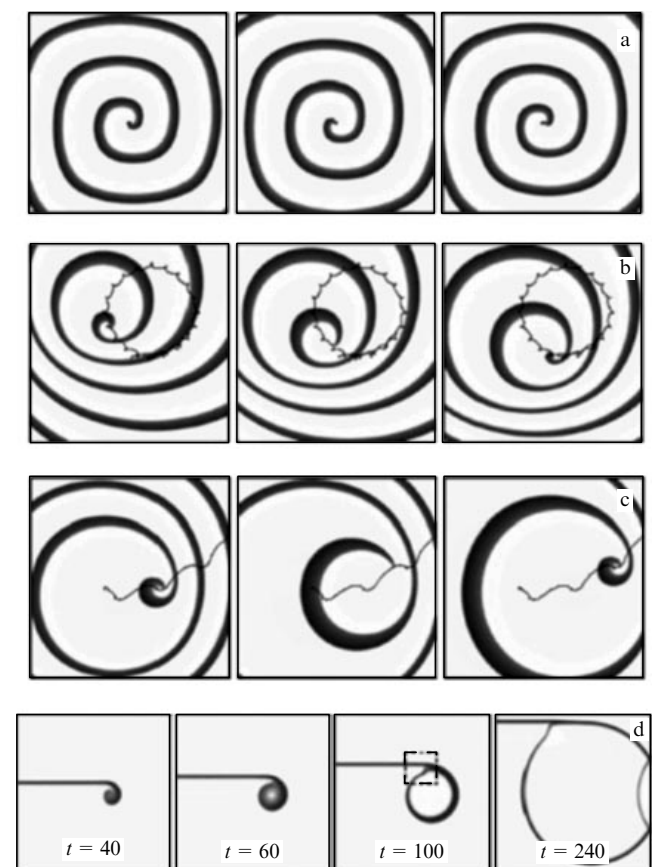


Figure 11. (a) Spiral wave in reaction–diffusion system (5): case (A), $L_x \times L_y = 200 \times 200$, $h_- = h_+ = 0$, $\Delta t = 150$; (b) Meander of the spiral with a small taxis coefficient: case (A), $L_x \times L_y = 200 \times 200$, $h_- = h_+ = 0.05$, $\Delta t = 400$; (c) Spiral behavior at higher taxis coefficients: case (A), $L_x \times L_y = 200 \times 200$, $h_- = h_+ = 0.1$, $\Delta t = 225$; (d) Wavebreak does not lead to the formation of a spiral wave: case (B), $L_x \times L_y = 250 \times 250$, $h_- = 5$, $h_+ = 1$.

Even these small taxis coefficients substantially change the behavior of the spiral and give rise to a spiral wave meander that drifts along a certain trajectory [70]. Such nonstationary behavior of spiral waves is unknown in excitable media, where the transition from steady rotation is usually associated with a change in reaction parameters. Conversely, in the case under consideration, such transition occurs upon a change in spatial parameters. As the taxis coefficients increase, they have a greater effect on wave spiral dynamics and the spiral wave meander extends such that the spiral drifts out of the medium and annihilates at its boundary (Fig. 11c).

4.2 Alternative behavior of wavebreaks

In autowave systems, a wavebreak leads to ‘germination’ of the tip and its curling up into a spiral wave if the medium is ‘strongly excitable’ or to shrinking (retraction) of the tip if the medium is ‘weakly excitable.’ Figure 11e presents an example of a reaction–taxis system where nothing of the kind takes place. This phenomenon also distinguishes taxis waves from classical autowaves. The broken tip of a taxis wave germinates but does not curl into a spiral, i.e., a qualitatively new phenomenon develops [70]. Germination of the wavebreak (WB) tip and transition to an expanding circle occur when $h_- > h_+$. The prey near the wavebreak have the capacity to escape from the predators into a region relatively free from them. In this region, the prey density increases due to reproduction, and an expanding circular zone forms where there is no chasing wave of predators and the prey density is rather high. However, the high-prey state ends when predators start to multiply intensively, giving rise to a chasing wave. The WB tip cannot be identified from the prey (P) population distribution, but a WB can be formally defined as an intersection of P and Z isolines [70]. This WB is attached to the ‘mother’ wave. This cannot happen in excitable reaction–diffusion systems because of a refractory period behind the excitation wave. The refractory period in the population system under consideration is characterized by a high density of predators such that triggering of the prey-escape mechanism is not feasible. Equilibrium between the variables P and Z behind the wave is reached very quickly (due to positive taxis of Z in the gradient of P); this marks a qualitative difference between taxis waves and classical autowaves. As a result, a taxis wave has a relatively short refractory tail (if any), which allows attraction and attachment of a WB to the back front of its own wave [70]. We note that the attached WB has to move much faster than a plane solitary wave because it simultaneously participates in the motion of the mother wave and the circular wave that moves at an angle to the mother wave. One reason for such faster motion is an unusual nonlinear dispersive coupling of taxis waves, whose velocity increases as the period decreases.

This property is illustrated in Fig. 12, which shows the velocity of waves propagating over a one-dimensional interval with periodic boundary conditions. Calculations were performed as follows. Initially, a wave was started on an interval of a large length L ; the interval ends then interlocked and the wave propagated circumferentially. The length L was then decreased in small steps, and the stationary velocity $v(L)$ was estimated after each step. To circumvent the interpretational difficulty related to the difference in spatial scales in the diffusion and taxis terms, we plotted not the absolute velocity but the velocity relative to the velocity of a solitary wave, $v(\infty)$.

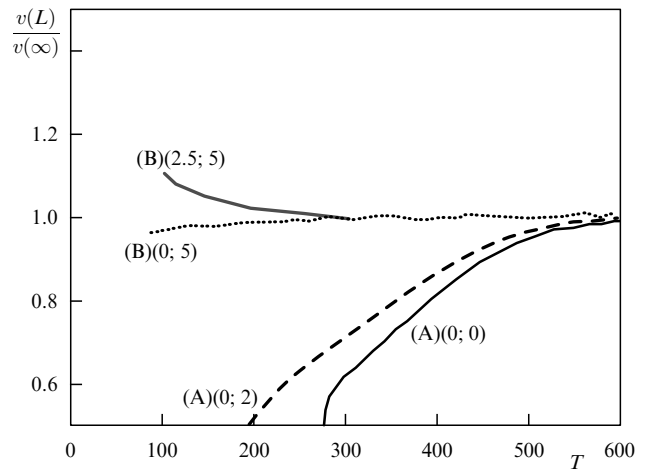


Figure 12. Dispersion curves of periodic waves as the dependence of the normalized velocity $v(L)/v(\infty)$ on the period $T = L/v(L)$ in cases (A) and (B) for different parameters (h_- and h_+ values are given in brackets). Reaction–diffusion waves decelerate as the frequency increases; the taxis wave can accelerate [70].

4.3 Partial reflection and self-supporting activity

In the one-dimensional case, taxis waves are reflected from the boundaries and penetrate through one another. In two dimensions, there are new aspects characterizing the impact of the waves with boundaries and with each other: the curvature of the waves and the angle of incidence at the instant of impact. It is shown in [70] that in reaction–taxis model (5), the curvature and/or the angle of incidence markedly affect the result of the impact, i.e., whether the wave is reflected from the medium boundary or is annihilated at it. An example is presented in Fig. 13a. A circular wave was initiated at an asymmetrically located site within a rectangular domain such that the distances to all boundaries were different. As a result, the wave annihilated at the ‘northern’ and ‘western’ boundaries (except for small portions) but was reflected from the ‘southern’ and ‘eastern’ ones. The wave approached the northern and western boundaries while having a greater curvature than when it reached the southern and eastern boundaries. The waves reflected from the southern and eastern boundaries partly annihilated on collision. Transition from annihilation to reflection/penetration depended on the wave front interaction angle. One more important factor that affected the outcome of the collision proved to be the ‘age’ of the propagating wave. This property of taxis waves is considered at greater length in the next section.

Thus, colliding waves either annihilate or penetrate/reflect, depending on the local details of their interaction; these two phenomena can work together to generate a self-supporting spatio-temporal activity. The typical sequence of events is as follows. Partially reflected/penetrated waves are broken, i.e., have free ends that do not curl up into spirals but produce circular waves. These waves interact with each other and with the medium boundaries, and therefore the sequence of events repeats, resulting in spatio-temporal chaos. Examples of such self-supporting activity are shown in Fig. 13b, c. Reference [70] presents a broad collection of numerical experiments demonstrating that this mechanism is not restricted to a narrow region of parameters. The self-supporting activity may last quite long but not necessarily infinitely long because there is always a possibility that all

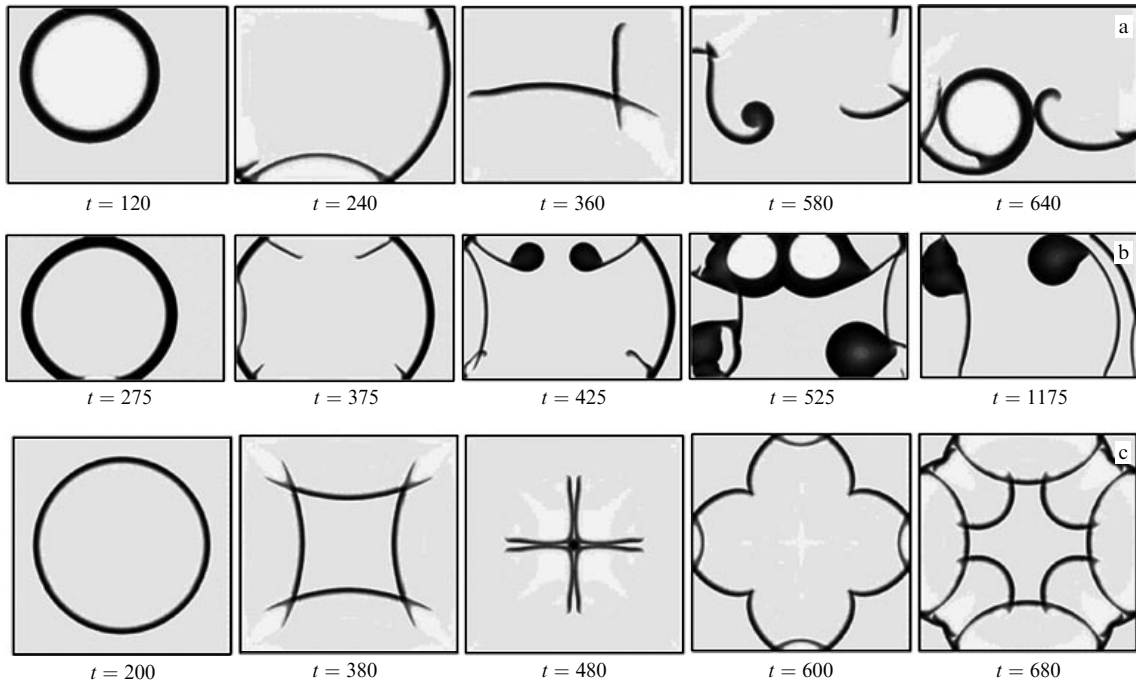


Figure 13. Self-supporting activity [70]. (a) Evolution of a circular wave: case (B), $L_x \times L_y = 200 \times 160$, $h_- = 5$, $h_+ = 1$; some parts are reflected from the boundaries, others are not; (b) case (A), $L_x \times L_y = 350 \times 230$, $h_- = 2$, $h_+ = 1.5$; (c) symmetric case (B), $L_x \times L_y = 250 \times 250$, $h_- = 5$, $h_+ = 1$.

waves annihilate on collision. Evidently, such probability is higher for a smaller system. At the same time, breaks resulting from partial reflection of the waves and formation of circular waves from their free ends may constitute a new mechanism underlying generation of spatio-temporal chaos.

5. Half-soliton interactions between population taxis waves

The results presented in this section were obtained in numerical experiments designed to study mathematical models (3) and (5) [71]. In the one-dimensional case, the implicit upwind difference scheme [69] was used with discretization steps $\delta x = 0.1$, $\delta t = 5 \times 10^{-3}$; in the two-dimensional case, the explicit upwind difference scheme with $\delta x = \delta y = 0.5$ and $\delta t = 5 \times 10^{-3}$ was used. As in the preceding sections, $\beta = 1$, $v = 0.07$, $w = 0.004$ for two different values of γ : $\gamma = 0.01$ and $\gamma = 0.016$. The Neumann condition $\partial P / \partial x|_{x=0,L} = 0$, $\partial Z / \partial x|_{x=0,L} = 0$ was satisfied in the one-

dimensional case ($x \in [0, L]$) and $\partial P / \partial x|_{x=0,L_x} = 0$, $\partial Z / \partial x|_{x=0,L_x} = 0$, $\partial P / \partial y|_{y=0,L_y} = 0$, $\partial Z / \partial y|_{y=0,L_y} = 0$ in the two-dimensional case ($(x, y) \in [0, L_x] \times [0, L_y]$).

5.1 One-dimensional case

It was shown in [71] that taxis waves have one more unique property, ‘half-soliton’ interaction, during which one colliding wave annihilates and the other continues to propagate. Figure 14a, b illustrates the spatio-temporal dynamics of solitary population taxis waves in model (3), including their formation, propagation, and reflection from the boundaries. These waves were initiated with $\gamma = 0.01$ (Fig. 14a) and $\gamma = 0.016$ (Fig. 14b) with the initial conditions $P(x, 0) = 0.8$ for $x \in [0, 1]$, $P(x, 0) = P_0$ for $x \in (1, L]$, and $Z(x, 0) = Z_0$ for $x \in [0, L]$, where P_0 and Z_0 are stationary values.

The results presented below are related to the following fact: the structure of a taxis wave and its propagation velocity are established after a rather long transitional period [71]. Figure 15A shows plots of the wave propagation velocity (V)

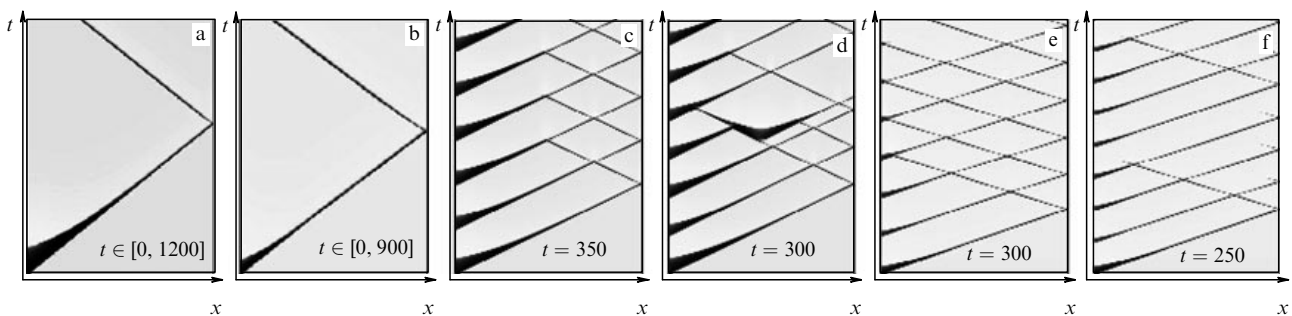


Figure 14. Spatio-temporal dynamics of one-dimensional ($L = 250$) taxis waves (3) with reflection from impenetrable boundaries [71]. Cases (a, b) — solitary waves, (c–f) — periodically initiated waves at the left end with period T and $t \in [0, 2000]$: (a) $\gamma = 0.01$, $D = 0.04$, $h_- = h_+ = 1$, (b), $\gamma = 0.016$, $D = 0$, $h_- = 5$, $h_+ = 1$, (c, d), $\gamma = 0.01$, $D = 0.04$, $h_- = h_+ = 1$, (e, f) $\gamma = 0.016$, $D = 0$, $h_- = 5$, $h_+ = 1$. Bold dark initial sections of the lines correspond to $P = 0.9$; thin dotted lines correspond to $P = 0$.

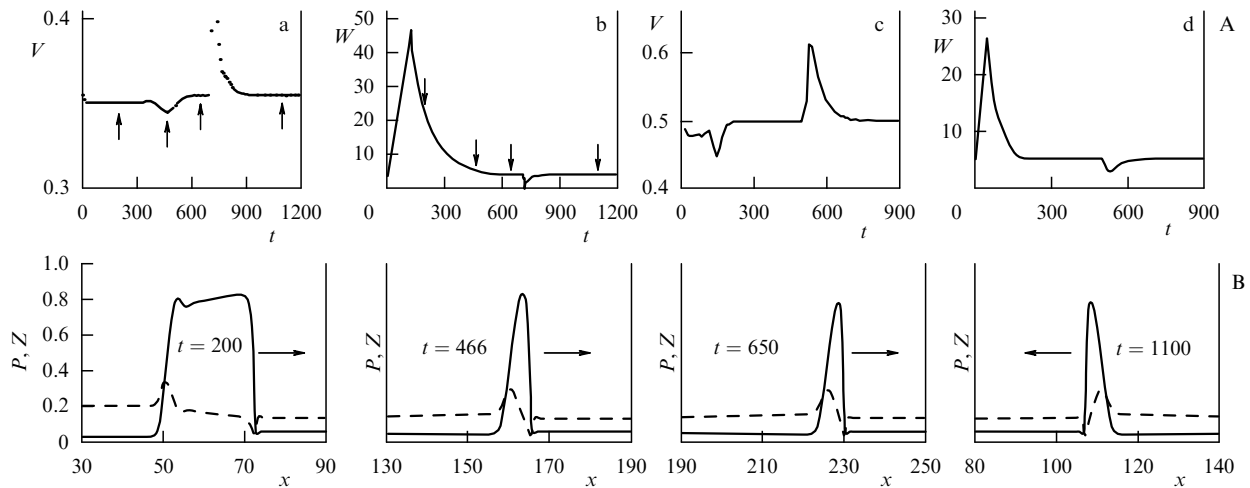


Figure 15. (A) Wave propagation velocity (a, c) and wave profile width (b, d) in the course of their establishment corresponding to 14a, b [71]: (a, b) $\gamma = 0.01, D = 0.04, h_- = h_+ = 1$, (c, d) $\gamma = 0.016, D = 0, h_- = 5, h_+ = 1$. The wave profile width $W(t)$ is defined as the distance between the points of the forward and rear fronts, where $P(x, t) = 0.4$. (B) Wave profiles corresponding to the chosen time instants t (arrows in Fig. A).

and the wave profile width (W) during such transition prior to and after reflection from the boundaries. In the course of establishment, the wave propagation velocity decreases sharply within a short time period (approximately $450 < t < 550$), whereas the wave profile width monotonically approaches a stationary value. The decrease in the velocity with time is associated with a change in the wave profile shape (see Section 3). Figure 15B shows wave profiles corresponding to the chosen time instants indicated by arrows in Fig. 15A. It can be seen that a temporary decrease in the velocity correlates with a change in the wave profile from ‘two-humped’ to ‘one-humped.’

On the other hand, the type of interaction of steadily propagating waves, i.e., reflection or annihilation, also correlates with the shape of their profile (see Section 3). Because the profile shape takes a rather long time to change after the initiation, it was suggested that the ‘age’ of the wave must affect the interaction regime. This suggestion was verified in numerical experiments presented in Figs 14c–f. Periodic waves were initiated in a one-dimensional medium with impenetrable boundaries. The figure illustrates interaction of the waves moving out from the left end of the section with those reflected from the impenetrable boundary. Two types of interaction occur, quasi-soliton and those in which

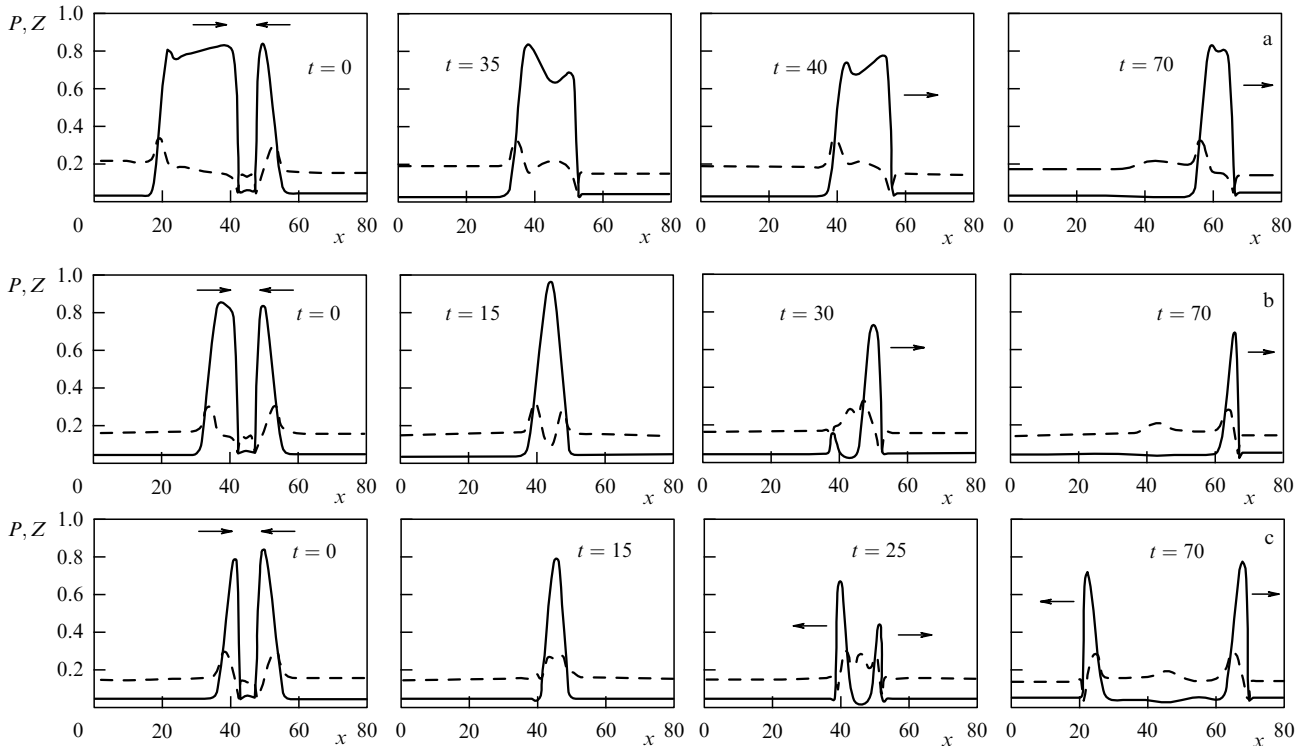


Figure 16. Results of collisions of differently ‘aged’ waves [71]: (a) waves W_{200} (left) and W_{466} (right); (b) waves W_{350} (left) and W_{466} (right); (c) waves W_{650} (left) and W_{466} (right).

only one wave passes after the collision; the latter represent a new type (half-soliton interactions).

Waves of different ‘ages’ were generated to study this phenomenon. They were recorded in a large system at given instants during transition to the stationary propagation regime, namely, at $t = 195, 345, 461,$ and 645 . Thereafter, the initial conditions were chosen such that half of the medium was occupied by a wave of one age shifted along the x axis and the other half by a wave of a different age turned toward the former one. Artificial starting conditions were such that the waves collided in roughly five time units; wave ages at the collision were as shown in Fig. 15. These waves are denoted as $W_{200}, W_{350}, W_{466},$ and W_{650} in the order of increasing age.

Figure 16a shows the interaction between waves W_{200} and W_{466} in which W_{200} suppresses W_{466} . Similarly, the wave W_{350} in Fig. 16b prevails over the wave W_{466} . Interaction between W_{650} and W_{466} occurs in the quasi-soliton regime. Tables 2 and 3 summarize the results of collisions of waves of different ages. It follows that half-soliton interaction occurs when two colliding waves have substantially different profile widths. It is more difficult for a narrow (‘old’) wave to penetrate through a wide (‘young’) wave.

Table 2. Results of taxis wave collisions for $\gamma = 0.01, D = 0.04, h_- = h_+ = 1$.

	A	B	C	D
A	–	A	A	A
B	A	+	B	B
C	A	B	+	+
D	A	B	+	+

Note: A corresponds to W_{200} , B to W_{350} , C to W_{466} , and D to W_{650} . Letters at the intersection of lines and columns indicate which wave suppresses the other; the + sign corresponds to the quasi-soliton regime, the – sign to annihilation. Wave profile ratios at the level $P = 0.4$: $\lambda_A/\lambda_D = 5.3, \lambda_B/\lambda_D = 2,$ and $\lambda_C/\lambda_D = 1.25$ [71].

Table 3. Results of taxis wave collisions for $\gamma = 0.016, D = 0, h_- = 5, h_+ = 1$ (Fig. 15c, d).

	a	b	c	d
a	–	a	a	a
b	a	–	b	b
c	a	b	+	+
d	a	b	+	+

Note: A corresponds to w_{84} , b to w_{140} , c to w_{160} , and d to w_{450} . Wave profile ratios at the level $P = 0.4$: $\lambda_a/\lambda_d = 2.8, \lambda_b/\lambda_d = 1.4,$ and $\lambda_c/\lambda_d = 1.14$ [71].

5.2 Two-dimensional medium

We consider the interaction between concentric taxis waves of different radii and profile widths [71]. In a one-dimensional collision, the initial conditions were formed by single pulses recorded at different stages of taxis wave development and therefore having different widths. If $P_{1d}(x), Z_{1d}(x)$ is the recorded impulse shifted along the x axis such that the front occurs at the point $x = 0$, the initial conditions used can be represented in the form

$$P(x, y, 0) = P_{1d}(\sqrt{x^2 + y^2} - R),$$

$$Z(x, y, 0) = Z_{1d}(\sqrt{x^2 + y^2} - R),$$

where R is the fixed radius of a circular wave.

This transformation for the parameters $\gamma = 0.016, D = 0, h_- = 5, h_+ = 1$ initiated circular waves from a one-dimensional wave taken at $t = 120$ (W-wave), $t = 450$ (S-wave), and $t = 450$ (U-wave). The profile widths of these waves measured at the level $P = 0.4$ were $\lambda_W = 9.2, \lambda_S = 6.4, \lambda_U = 5.1,$ and hence $\lambda_W/\lambda_U = 1.8$ and $\lambda_S/\lambda_U = 1.25$.

Interaction of U-waves with the initial radius $R = 35$ is shown in Fig. 17a. In this case, both waves penetrate through (reflect from) each other and undergo reflection from the boundaries. Interaction of U and W-waves with the same radii exhibits half-soliton behavior whereupon the W-wave suppresses the U-wave but annihilates at the boundary (Fig. 17b).

5.3 Taxitons. Dependence of the reflection regime on the taxis wave interaction angle

The collision of two S-waves with the initial radius $R = 20$ (Fig. 17b) results in their partial penetration. The result is given by spatially localized waves called ‘taxitons,’ analogous to the term ‘excitons’ [154] coined to describe localized propagating excitations in excitable media [71] (Fig. 17c, $t = 80$).

In certain cases, two regimes, half-soliton and taxiton, are simultaneously realized after collision (Fig. 17d). When a U-wave ($R = 35$) interacts with an S-wave ($R = 20$), the latter passes through the former in the half-soliton regime, whereas a U-wave passes only partially through (Fig. 17d, $t = 60, 80, 100$).

The interaction type (annihilation, quasi-soliton, or half-soliton) depends not only on the curvature of the colliding waves and the width of their profiles but also on the incidence angle [71]. This explains the formation of taxitons.

Figure 18 shows collisions of plane taxis waves at different angles between interacting fronts. The initial conditions were formed by a stationary one-dimensional U-wave converted to a pair of two-dimensional plane waves propagating in opposite directions with different tilts. The following transformation was used for the purpose:

$$P(x, y, 0) = P_{1d}(x \cos \theta + y \sin \theta - C),$$

$$Z(x, y, 0) = Z_{1d}(x \cos \theta + y \sin \theta - C),$$

where θ and C are constants that differ for the right and left halves of the medium.

As a result, the waves annihilate when the angle between their interacting fronts is $\alpha = 80^\circ$ (Fig. 18a) and pass through each other at $\alpha = 60^\circ$ (Fig. 18b).

6. Waves in excitable media with linear cross-diffusion

6.1 Examples of systems with cross-diffusion

In the preceding sections, we considered mathematical models with taxes that can be classified as nonlinear cross-diffusion ones. The number of publications devoted to systems with linear cross-diffusion is relatively small compared to publications on nonlinear cross-diffusion.

In 1975, Jorné [20] demonstrated in the context of chemical reactions (dynamics of electrolyte solutions) that the introduction of negative linear cross-diffusion in the reaction–diffusion equations enhances the probability of instabilities leading to oscillations and the formation of

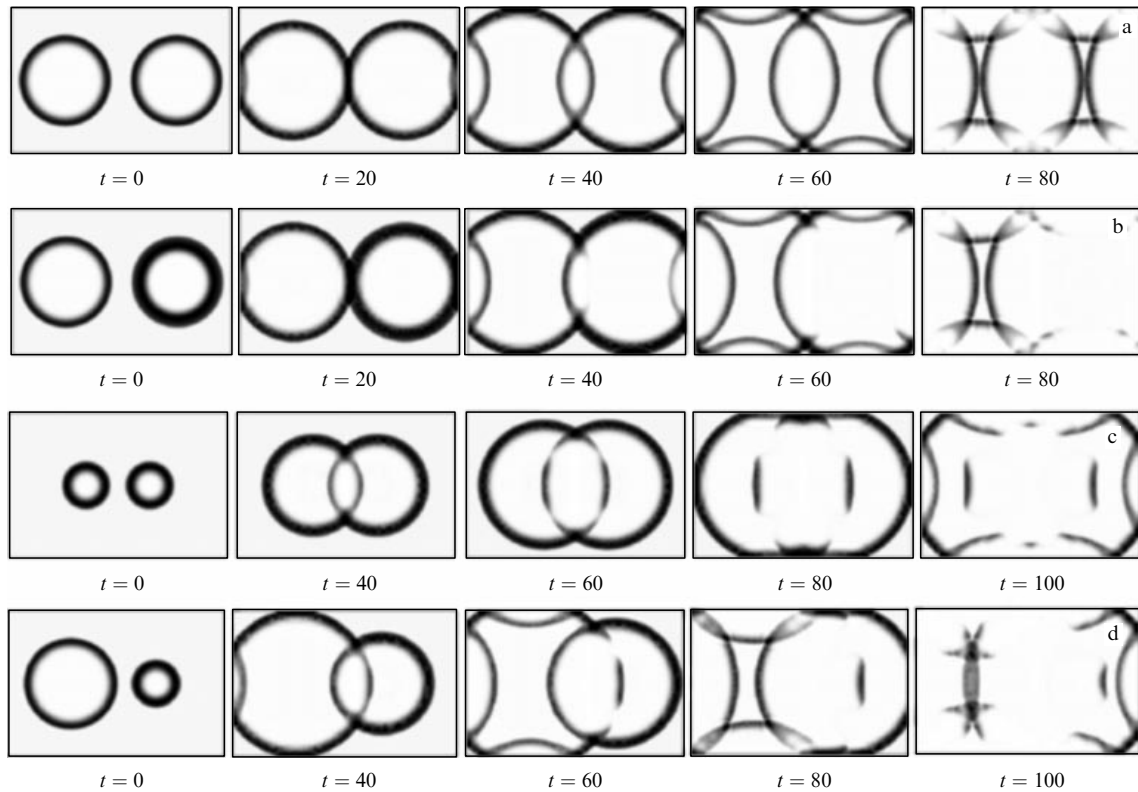


Figure 17. Interaction of concentric taxis waves ($L_x \times L_y = 150 \times 100$) [71]; (a) quasi-soliton interaction of U-waves with initial radii $R = 35$; (b) half-soliton interaction of U- and W-waves with $R = 35$; (c) two S-waves with $R = 20$; (d) U-wave ($R = 35$) and S-wave ($R = 20$).



Figure 18. Interaction of two plane U-waves at different angles α between the fronts ($L_x \times L_y = 150 \times 50$, $\Delta t = 20$) [71]: (a) $\alpha = 80^\circ$, (b) $\alpha = 60^\circ$.

ordered structures. In a later study, the same author examined the Lotka – Volterra equation with diffusion in a homogeneous system encompassing negative linear cross-diffusion [155]. He observed the appearance of oscillations and spatial structures at certain values of cross-diffusion coefficients. Since then, negative cross-diffusion has been recognized as a factor responsible for unstable regimes in the extended Lotka – Volterra system [45, 46, 156].

Satulovsky [156] also used the Lotka – Volterra system to study the behavior of predators and prey that led to equations with negative cross-diffusion. Jorné [155] and Satulovsky [156] emphasized that negative cross-diffusion considered in their works is rarely applicable to ecological situations because it reflects a detrimental behavioral strategy on the part of the prey.

Almirantis and Papageorgiou [21] postulated a mechanism of intercellular communication capable of maintaining cross-diffusion transport in biological systems. As an illustration, they proposed a hypothetical membrane mechanism including transmembrane microstructures with enzymatic activity having two active and one regulatory

sites. It turned out that at such spatial relations, a simple catalytic reaction (even with very low cross-diffusion compared with ordinary diffusion) can yield structures. The same authors [21] also studied the reaction – cross-diffusion system

$$\begin{aligned} \frac{\partial}{\partial t} X &= F(X, Y, A) + D_X \frac{\partial^2}{\partial r^2} X + D_{XY} \frac{\partial^2}{\partial r^2} Y, \\ \frac{\partial}{\partial t} Y &= G(X, Y, A) + D_Y \frac{\partial^2}{\partial r^2} Y + D_{YX} \frac{\partial^2}{\partial r^2} X, \end{aligned} \tag{7}$$

where X and Y are regulatory and ‘transport’ substances, respectively.

Conditions were found at which stationary structures could form in the two-component reaction – diffusion system (7) in the presence of cross-diffusion. In other words, the authors of Ref. [21] proposed and investigated a hypothetical mechanism involving transmembrane allosteric enzymes as a possible candidate for the creation of a cross-diffusion interaction between components of the system in which dissipative structures arise. Some characteristics of mem-

brane microstructures reported in that paper were observed in certain receptor systems [157, 158].

Dubey and collaborators [24] considered the following predator – prey model with self- and cross-diffusion:

$$\begin{aligned} \frac{\partial P}{\partial t} &= g(P)P - f(P)Z + D_{11} \frac{\partial^2 P}{\partial x^2} + D_{12} \frac{\partial^2 Z}{\partial x^2}, \\ \frac{\partial Z}{\partial t} &= [cf(P) - q(P)]Z + D_{22} \frac{\partial^2 Z}{\partial x^2} + D_{21}(t) \frac{\partial^2 P}{\partial x^2}, \end{aligned} \tag{8}$$

where $P(x, t)$ and $Z(x, t)$ are prey and predator population densities, respectively. This model was used to study instability and global stability criteria, as well as the effect of critical wavelength, which may bring a cross-diffusion system to unstable regimes. Also considered was the case of a time-dependent predator’s cross-diffusion coefficient; the effect of time-dependent cross-diffusion on the stability of the system was evaluated [24].

Seismology. Burridge – Knopoff model (BK model). Burridge and Knopoff [28] proposed describing characteristic features of earthquakes using a model that considers the interaction of two tectonic plates as the interaction of a chain of N blocks of equal length a and mass m interconnected by springs with Hooke’s coefficient k_c . The blocks are attached to the main part of a plate moving with speed V . The connection of the blocks with this plate is determined by an elastic shift with a coefficient k_p and friction F_f between the two plates. In the stationary state, the equation for the i th block has the form

$$m\dot{X}_i = k_c(X_{i+1} - 2X_i + X_{i-1}) - k_p(X_i - Vt) - F_f(\dot{X}_i), \tag{9}$$

where X_i is the displacement of the i th block from equilibrium. Burridge and Knopoff [28] introduced an S -shaped dependence of the friction function. In further studies, Carlson and Langer [159, 160] introduced a friction function asymptotically decaying with increasing velocity. Cartwright and collaborators [29] returned to the initial shape of the friction function and reduced the BK model to a system with linear cross-diffusion.

Passing to the limit in Eqn (9), we have

$$\ddot{\chi} = c^2\chi'' - (\chi - vt) - \gamma\varphi(\dot{\chi}), \tag{10}$$

where $\chi(x, t)$ is the time-dependent local lengthwise displacement of the upper plate relative to the lower one. For the local velocity $\psi = \dot{\chi}$, Eqn (10) gives a BK model in the form of a system with linear cross-diffusion [29]:

$$\dot{\psi} = \gamma(\eta - \varphi(\psi)), \quad \dot{\eta} = -\gamma^{-1}(\psi - v - c^2\psi''). \tag{11}$$

Cross-diffusion model of forest-age structure dynamics. From the mathematical standpoint, systems with linear cross-diffusion appear to be simpler than those with nonlinear cross-diffusion; however, their physical representation presents difficulty. We consider one of the most interesting corollaries of a mathematical model with linear cross-diffusion using the model of forest-age structure dynamics proposed in [26, 27]. Forest-age structure dynamics is understood as a change in the number of trees of different age classes in space and time under the effect of internal and external factors. The age structure of natural forests varies from one place to another, and such ‘cells’ are integrated into a common system by mechanisms of seed dispersal and

vegetative reproduction. Trees are known to reproduce themselves by seeds via four main stages: seed production, seed transport, seed deposition on the soil, and germination. The following model was considered:

$$\begin{aligned} \frac{\partial u}{\partial t} &= \delta\beta w - \gamma(v)u - fu, \\ \frac{\partial v}{\partial t} &= fu - hv, \\ \frac{\partial w}{\partial t} &= \alpha v - \beta w + Dw_{xx}, \end{aligned} \tag{12}$$

where u and v are the density of ‘young’ and ‘old’ trees; w is the seed density in ‘the air’, f and h are the aging coefficient of ‘young’ and mortality coefficient of ‘old’ trees, respectively; $\gamma(v)$ is the mortality of young trees; α , β , and δ are the respective coefficients of seed production, deposition, and germination; and D is the coefficient of diffusion along the spatial variable x . System (12) looks like a reaction – diffusion one. Elimination of the ‘seed’ variable from (12) yields a cross-diffusion system of equations for the density of young and old tree classes [26, 27].

The cross-diffusion model in [26, 27] was derived based on the hypothesis of different timescales for seed dispersion and tree lifetimes. Because the last equation in system (12) is linear, its formal solution can be written as

$$\begin{aligned} w(x, t) &= \int_{-\infty}^{+\infty} d\xi \int_0^{+\infty} d\tau v(x + \xi, t - \tau) \\ &\quad \times \frac{\alpha}{2\sqrt{\pi D\tau}} \exp\left(-\frac{\xi^2}{4D\tau} - \beta\tau\right). \end{aligned} \tag{13}$$

It should be borne in mind that the time spent by seeds in the air is much smaller than all other time-dependent constants; in other words, β^{-1} (the characteristic seed deposition time) is a small parameter. Expansion of v in a Taylor series in the second argument gives an asymptotic series for w in the limit $\beta \rightarrow +\infty$:

$$\begin{aligned} w(x, t) &= \int_{-\infty}^{+\infty} d\xi \left\{ v(x + \xi, t) \int_0^{+\infty} d\tau \frac{\alpha}{2\sqrt{\pi D\tau}} \right. \\ &\quad \times \exp\left(-\frac{\xi^2}{4D\tau} - \beta\tau\right) + v_t(x + \xi, t) \int_0^{+\infty} d\tau \frac{\alpha}{2\sqrt{\pi D\tau}} \\ &\quad \times \exp\left(-\frac{\xi^2}{4D\tau} - \beta\tau\right) + \dots \left. \right\} \\ &= \alpha \int_{-\infty}^{+\infty} d\xi \left\{ v(x + \xi, t) \frac{1}{\sqrt{D\beta}} \exp\left[-|\xi| \left(\frac{\beta}{D}\right)^{1/2}\right] \right. \\ &\quad + v_t(x + \xi, t) \frac{1}{2\sqrt{D\beta^3}} \left[1 + |\xi| \left(\frac{\beta}{D}\right)^{1/2}\right] \\ &\quad \times \exp\left[-|\xi| \left(\frac{\beta}{D}\right)^{1/2}\right] \left. \right\} + O(\beta^{-5/2}). \end{aligned} \tag{14}$$

Substitution of this expression in the first equation of system (12) (keeping only the leading term) leads to the integro-differential set of equations

$$\begin{aligned} u_t &= \int_{-\infty}^{+\infty} \rho_0(\xi) v(x + \xi, t) d\xi - \gamma(v)u - fu, \\ v_t &= fu - hv, \end{aligned} \tag{15}$$

where the function ρ_0 is given by the formula

$$\rho_0(\xi) = \alpha\delta \left(\frac{\beta}{D}\right)^{1/2} \exp\left[-|\xi| \left(\frac{\beta}{D}\right)^{1/2}\right]. \quad (16)$$

The integral term in (15) can be approximated by a differential one if $v(x + \xi)$ is expanded in a Taylor series and only the first four terms are retained. This approach has no rigorous substantiation, but it gives the first ‘nontrivial’ spatially extended generalization of model (12). The assumption that

$$\int_{-\infty}^{+\infty} \rho_0(\xi) v(x + \xi, t) d\xi \cong \rho v(x, t) + K v_{xx}(x, t),$$

where

$$\rho = \int_{-\infty}^{+\infty} \rho_0(\xi) d\xi = 2\alpha\delta,$$

$$K = \frac{1}{2} \int_{-\infty}^{+\infty} \rho_0(\xi) \xi^2 d\xi = \frac{2\alpha\delta D}{\beta},$$

leads to the following system with cross-diffusion:

$$\frac{\partial u}{\partial t} = \rho v - \gamma(v)u - fu + K v_{xx},$$

$$\frac{\partial v}{\partial t} = fu - hv. \quad (17)$$

The linear and cubic terms in ξ disappear due to the parity of ρ_0 . We note that system (17) already has a cross-diffusion term $K v_{xx}$, whereas model (12) includes the classical diffusion term $D w_{xx}$. To conclude, a cross-diffusion model with two interacting components was proposed to describe spatio-temporal dynamics of the age structure of monospecific forest stands [26, 27]. In addition, tree limit displacement was examined in [26, 27] in the context of model (17).

6.2 Characteristic wave properties

Mathematical model. It was shown in [72] that a characteristic property of waves in excitable systems with linear cross-diffusion is their quasi-soliton interaction regime. This study used a mathematical model with the FitzHugh–Nagumo nonlinearity [142, 143], a prototype of an excitable system model including linear cross-diffusion (19) instead of the traditional description of the system component distribution through diffusion (18) [72]:

$$\frac{\partial u}{\partial t} = u(u - a)(1 - u) - v + D_u \frac{\partial^2 u}{\partial x^2},$$

$$\frac{\partial v}{\partial t} = \varepsilon(u - v) + D_v \frac{\partial^2 v}{\partial x^2}, \quad (18)$$

$$\frac{\partial u}{\partial t} = u(u - a)(1 - u) - v + D_v \frac{\partial^2 v}{\partial x^2},$$

$$\frac{\partial v}{\partial t} = \varepsilon(u - v) - D_u \frac{\partial^2 u}{\partial x^2}, \quad (19)$$

where $D_u \geq 0, D_v \geq 0, \varepsilon \ll 1, a < 0.5$.

The signs of cross-diffusion terms in (19) were chosen analogously to the studied system with nonlinear cross-diffusion. It is worth noting that system (19) at $D_v = 0$ corresponds to the Burridge–Knopoff model describing the interaction of tectonic plates [29].

Numerical experiments with system (19) were carried out for $x \in [0, L]$, where the medium size L varied in different cases. The impenetrability conditions $\partial u/\partial x|_{x=0, L} = \partial v/\partial x|_{x=0, L} = 0$ were satisfied at the boundaries of the medium. Whenever wave behavior in an unbounded medium had to be examined, the computation interval was from time to time displaced so as to exclude the boundary effect on wave propagation. For this reason, spatial coordinates in all figures represent a spatial scale rather than the wave position in a concrete experiment. In all numerical experiments, the parameter a was fixed as $a = 0.3$, whereas ε, D_u , and D_v were varied. The implicit central-difference scheme [161] was used for calculations. The spatial and temporal steps of calculations were $\delta x = 0.2$ and $\delta t = 0.005$. The initial conditions were chosen as $u(x, 0) = \Theta(\delta - x)$ and $v(x, 0) = 0$ for starting one wave (at the left end), and as $u(x, 0) = \Theta(\delta - x) + \Theta(x - (L - \delta))$ and $v(x, 0) = 0$ for starting two waves from either end, where Θ is the Heaviside function and $\delta = 2$. The beginning and end of the excitation wave were defined as the points where $u(x, t) = u_f = 0.5$.

Evolution of wave shape. Figure 19A depicts a typical profile of a wave traveling in the excitable cross-diffusion system (19). The following characteristic properties are worth noting [72]:

- a quite long transitional period (much longer than in a system with usual diffusion) during which a wave pulse expands to a certain stationary length;
 - an oscillating forefront of the pulse;
 - oscillations of the wave profile near the forward and back fronts are apparent for both the activator and the inhibitor;
 - the pulse plateaus (Fig. 19A, $t = 120, t = 620$) of both the activator and the inhibitor vary insignificantly.
- All these properties are reminiscent of those described for taxis waves and differ from wave properties in a FitzHugh–Nagumo system with ordinary diffusion:
- the transition to a stable pulse usually occurs for a time comparable with its duration;
 - the forward and back fronts are monotonic;
 - the soliton-like interaction regime is confined to a narrow parameter region at the boundary of the standby and oscillatory regimes.

We consider the evolution of a wave profile width W defined as the distance between the point where $u = u_f$ and $\partial u/\partial t > 0$ (forefront) and $u = u_f$ and the point where $\partial u/\partial t < 0$ (back front) at a given instant. Figure 19B shows that with the chosen initial conditions, the wave profile width increases to a stationary value. Both the stationary value of the profile width and its growth rate depend on all parameters. However, the ε -dependence appears especially interesting because the saturation effect is eliminated at $\varepsilon = 0$ [Fig. 19B (d)].

In Fig. 19C, it is possible to trace the wave shape evolution in detail at small values of the parameter ε . The wave becomes longer, which allows comparing the forward and back fronts better at different instants. If the two fronts are superimposed at $t = 250$ and $t = 1000$, the forefront remains practically constant during the prolonged wave transition to the stationary state [Fig. 19C (c)], whereas the rear front undergoes relatively small changes.

We separately consider the motion of the forward and back fronts in terms of variation of their velocities with time (Fig. 19D). It can be seen that the forefront velocity becomes

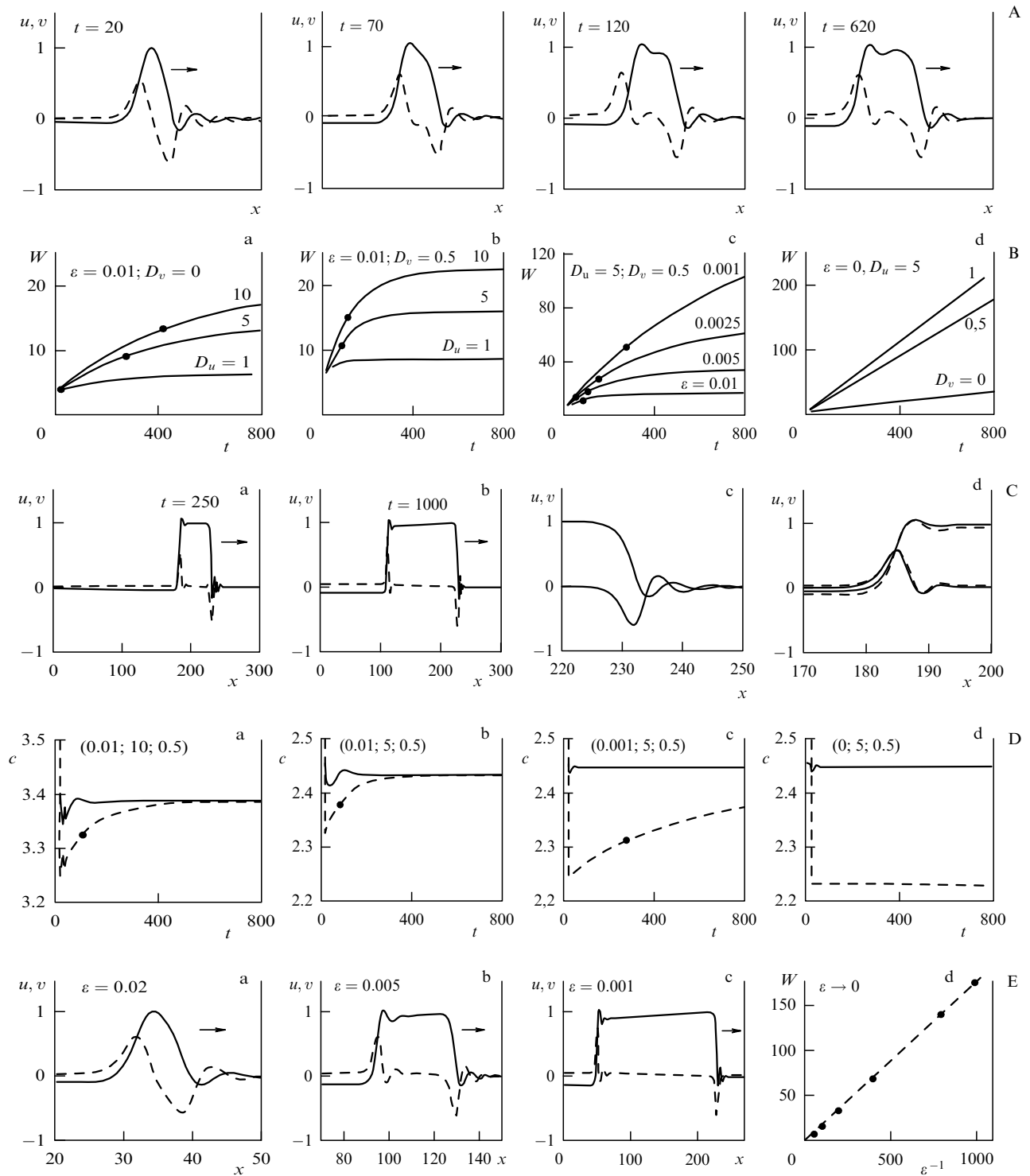


Figure 19. (A) Profile of a propagating wave described by mathematical model (19). Solid lines: u , dotted lines: v . Parameters: $\epsilon = 0.001, D_u = 5, D_v = 0.5$; the range of x is 50 in all figures. (B) Time-dependent growth of the wave profile width (W) at various combinations of system parameters (19). Points on the graphs denote boundaries of the quasi-soliton regime; the wave is reflected at the boundary if collision occurs before the indicated instant. The curve $D_u = 1$ in Fig. (b) — quasi-soliton regime is absent. Figure (d): $\epsilon = 0$, i.e. the quasi-soliton regime persisted throughout the period of observation. (C) Details of the wave shape evolution in time ($\epsilon = 0.001, D_u = 5, D_v = 0.5$): (a) and (b) general view; (c) superposition of forward fronts corresponding to instants $t = 250$ and $t = 100$; (d) superposition of rear fronts. (D) Speed evolution of forward (solid line) and back (dashed line) wave fronts in time at different combinations of the parameters ϵ, D_u, D_v (in parentheses at the top of the figures). Points on the graphs denote boundaries of the quasi-soliton regime; the wave is reflected at the boundary if collision occurs before the indicated instant. For $\epsilon = 0$ (d), the quasi-soliton regime persisted throughout the observation period. (E) Stable wave profiles for different values of the parameter ϵ . The stationary wave width W (Fig. 2) is proportional to ϵ^{-1} as $\epsilon \rightarrow 0$; points show results of numerical experiments. In all cases (Figs a–d), $D_u = 5$ and $D_v = 0.5$.

constant after a very short transitional period. In contrast, the back front velocity gradually increases from a very small value and needs rather a long period to reach the forefront

velocity. Thus, the dynamics of wave profile formation can be described as a gap distance between back and forward fronts at which the velocities of the two become equal. The change in

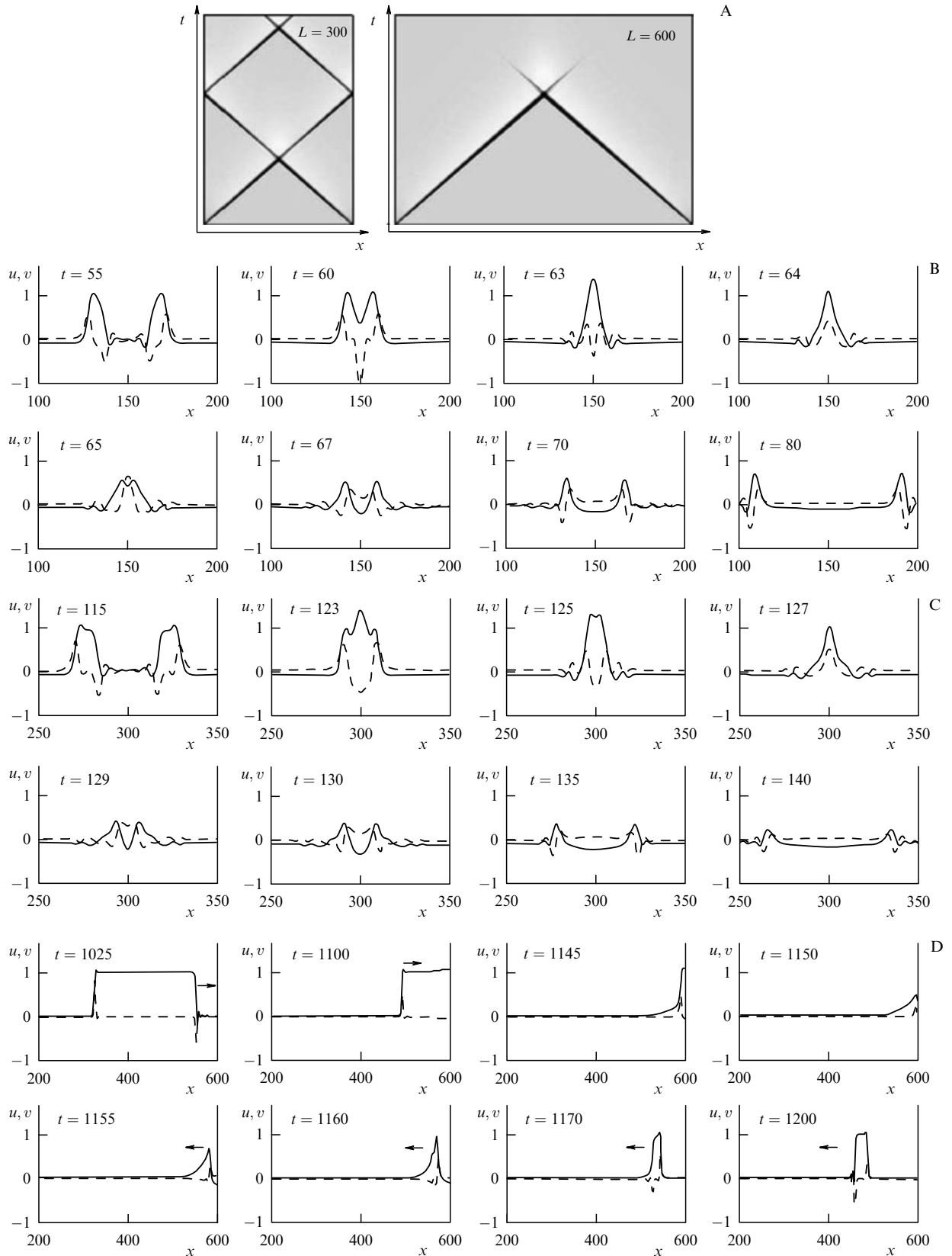


Figure 20. Wave interaction in an excitable system with linear cross-diffusion [72]. (A) Spatio-temporal patterns of the wave (u, v) interaction in one-dimensional media of different lengths L : a quasi-soliton regime in a small medium and the nonsoliton regime in a large medium. In either case, $t \in [0, 200]$. Parameters of system (19): $\varepsilon = 0.01$, $D_v = 0.5$. (B) Dynamics of the quasi-soliton wave interaction at $L = 300$ (solid lines: u , dashed lines: v). (C) Dynamics of the nonsoliton wave interaction at $L = 600$. (D) Quasi-soliton interaction of a wave with an impenetrable boundary at $\varepsilon = 0$. (In all cases, $D_u = 5$ and $D_v = 0.5$).

the back front velocity slows down as the value of ε decreases [Fig. 19D (a–c)], but it does not change at all at $\varepsilon = 0$

[Fig. 19D (d)]. Such divergence in the motion of the forward and back fronts accounts for the continuous growth of the

wavelength. Figure 19E illustrates the ε -dependence of stable wave profiles. At small ε , stable wavelengths W are fairly well approximated by the dependence $W \propto \varepsilon^{-1}$.

6.3 Quasi-soliton wave interaction

It was shown in [72] that quasi-soliton interaction is also a characteristic property of waves in excitable systems with cross-diffusion. This property is related to the slow evolution of the wave shape described in the preceding section. The ability of waves to penetrate through one another and reflect at impenetrable boundaries depends on their ‘age’, i.e., profile width at the moment of collision.

Figure 20A shows two interaction regimes for waves of different ages at identical parameters. Such waves were obtained by varying the medium size. In a smaller system ($L = 300$), wave profiles prior to the impact did not reach a proper width; hence, a quasi-soliton collision occurs. After the collision, the waves became narrow again and, as a consequence, were reflected from the boundaries during further propagation. This process repeated over and over, ensuring self-supporting activity of the system. In a larger system ($L = 600$), waves had wide enough profiles at the instant of impact and annihilated [72]. The dynamics of quasi-soliton and nonsoliton interactions between waves in both cases are shown in Fig. 20B, C. Similar to taxis waves, the nonsoliton interaction regime in the given case is characterized by wave penetration through one another and their subsequent decay.

Switching from a soliton-like to a nonsoliton interaction regime occurs when a wave is in a certain ‘expansion’ phase during transition to the stable state. The instants of this switch are shown in Figs 19B and 19D. The quasi-soliton interaction regime holds only for ‘narrow’ waves, i.e., for waves in the first half of the transition to the steady state (Fig. 19b). The wave profile width grows depending on the back front dynamics (i.e., on its spatial location and structure). Therefore, it may be supposed that the outcome of collision is largely determined by the back front properties. The interrelation between forward and back fronts must be negligible when the wave profile is very wide.

The structure of the rear part of a wide wave profile remains the same as in a narrow profile; that is, it is capable of reflection if the pulse plateau changes rather slowly, depending on the parameter ε . This suggestion was confirmed in numerical experiments (Fig. 19D(d)) [72]. The same work [72] describes an analytic approach to the study of waves in systems with linear cross-diffusion.

7. Conclusion

We have shown that the replacement of usual diffusion by cross-diffusion in excitable systems results in new wave properties.

The main properties and new wave phenomena characteristic of systems with cross-diffusion and distinguishing them from the known properties of autowaves are as follows.

- There is an oscillating forefront of waves in cross-diffusion systems.
- ‘One-humped’ or ‘two-humped’ wave profiles occur. The dependence of the wave propagation velocity on the taxis coefficients has two branches, parabolic and linear. The transition from one branch to the other fairly well correlates with changes in the wave profile shape; that is, the parabolic branch corresponds to the ‘two-humped’ shape and the linear branch to the ‘one-humped’ shape.

- There is a rather long transition (much longer than in a system with ordinary diffusion) during which a wave pulse reaches a certain stationary length.

- The dependence of the taxis wave propagation velocity on the diffusion coefficient differs from the \sqrt{D} dependence always present in reaction–diffusion systems.

- Small taxis coefficients substantially alter the behavior of spiral waves and lead to a spiral wave meander. Such nonstationary behavior of spiral waves is unknown in excitable reaction–diffusion systems, where the transition from steady rotation is usually associated with changes in the reaction parameters.

- Partial diffusion of cross-diffusion waves is possible in two-dimensional systems.

- Free tips of wavebreaks can attach to the back front of the mother wave, generating a circular wave.

- The quasi-soliton interaction regime associated with collisions of cross-diffusion waves spreads over a large parameter region. The soliton-like interaction regime in reaction–diffusion systems is confined to a very narrow parameter region at the boundary of standby and oscillating regimes.

- In the nonsoliton interaction regime in cross-diffusion systems, waves do not annihilate but always penetrate through one another and thereafter decay.

- The half-soliton interaction regime occurs under certain conditions in cross-diffusion systems.

- There is a relation between wave shape evolution and various wave interaction regimes (quasi-soliton, nonsoliton, and half-soliton).

These findings indicate that waves in excitable cross-diffusion systems may be regarded as a special class of nonlinear waves.

The present review was not designed to compare analytic approaches to the study of cross-diffusion systems. Such investigations were initiated by the publication of the Keller–Segel mathematical model in 1971 [124] describing chemotaxis in population systems. The majority of analytic works deal with self-organization processes in population systems (see, e.g., [9, 15, 25, 44, 155, 162–167]). It is worthwhile to mention the works of Talanov [168, 169], who proposed a phenomenological description of nonlinear cooperative effects in extended kinetic systems and analyzed the relation of stimulated diffusion (nonlinear diffusion and cross-diffusion) to the principles of thermodynamics. An asymptotic theory for the regime in which the local dynamics of the inhibitor is much smaller than that of the activator is suggested in Ref. [72]; it considers the classical FitzHugh–Nagumo system in which ordinary diffusion was substituted by linear cross-diffusion.

In the present work, the properties of waves in cross-diffusion systems are largely reviewed in application to spatially extended population systems for which selected mechanisms underlying the wave phenomena of interest can be explained. Moreover, a number of experimental data available for population systems confirm some wave properties discovered in mathematical models.

It can be expected that further theoretical and experimental studies of excitable systems with cross-diffusion will make an important contribution to understanding self-organization phenomena in all sorts of nonlinear systems, from micro- and astrophysical systems to social ones.

The authors are grateful to E E Shnol’ and O A Mornev for valuable comments. Financial support for the studies by

RFBR (grant 03-01-00673) and EPSRC (Grant No. GR/08664/01, UK) is acknowledged.

References

- Turing A M *Philos. Trans. R. Soc. London Ser. B* **237** 37 (1952)
- Haken H *Synergetics* (Berlin: Springer-Verlag, 1978) [Translated into Russian (Moscow: Mir, 1980)]
- Loskutov A Yu, Mikhailov A S *Vvedenie v Sinergetiku* (Introduction to Synergetics) (Moscow: Nauka, 1990); see also *Foundations of Synergetics* (Berlin: Springer-Verlag, 1990)
- Malinetskii G G *Matematicheskie Osnovy Sinergetiki: Khaos, Struktury, Vychislitel'nyi Eksperiment* (Mathematical Principles of Synergetics: Chaos, Structures, Numerical Experiment) 4th ed. (Moscow: Editorial URSS, 2005)
- Trubetskov D I *Vvedenie v Sinergetiku. Khaos i Struktury* (Introduction to Synergetics. Chaos and Structures) 2nd ed. (Moscow: Editorial URSS, 2004)
- Ivanitskii G R, Krinskii V I, Sel'kov E E *Matematicheskaya Biofizika Kletki* (Mathematical Biophysics of the Cell) (Moscow: Nauka, 1978)
- Polak L S, Mikhailov A S *Samoorganizatsiya v Neravnovesnykh Fiziko-khimicheskikh Sistemakh* (Self-Organization in Non-Equilibrium Physico-Chemical Systems) (Moscow: Nauka, 1983)
- Cross M C, Hohenberg P C *Rev. Mod. Phys.* **65** 851 (1993)
- Murray J D *Mathematical Biology* 3rd ed. (Berlin: Springer, 2002–2003)
- del-Castillo-Negrete D, Carreras B A, Lynch V *Physica D* **168–169** 45 (2002)
- Okubo A *Diffusion and Ecological Problems: Mathematical Models* (Biomathematics, Vol. 10) (Berlin: Springer-Verlag, 1980)
- Ivanitskii G R, Panfilov A V, Tsyganov M A *Biofizika* **32** 354 (1987)
- Kawasaki K et al. *J. Theor. Biol.* **188** 177 (1997)
- Kozlovsky Y et al. *Phys. Rev. E* **59** 7025 (1999)
- Mimura M, Sakaguchi H, Matsushita M *Physica A* **282** 283 (2000)
- Wakano J Y, Komoto A, Yamaguchi Y *Phys. Rev. E* **69** 051904 (2004)
- Samarskii A A et al. *Rezhimy s Obostreniem v Zadachakh dlya Kvazilineinykh Parabolicheskikh Uravnenii* (Regimes with Sharpening in Problems for Quasilinear Parabolic Equations) (Moscow: Nauka, 1987) [Translated into English: *Blow-up in Quasilinear Parabolic Equations* (Berlin: De Gruyter, 1995)]
- Akhmeeva T S *Nestatsionarnye Struktury i Diffuzionnyi Khaos* (Non-Stationary Structures and Diffusional Chaos) (Moscow: Nauka, 1992)
- del-Castillo-Negrete D, Carreras B A *Phys. Plasmas* **9** 118 (2002)
- Jorné J J. *Theor. Biol.* **55** 529 (1975)
- Almirantis Y, Papageorgiou S J. *Theor. Biol.* **151** 289 (1991)
- Ivanitskii G R, Medvinskii A B, Tsyganov M A *Usp. Fiz. Nauk* **161** (4) 13 (1991) [*Sov. Phys. Usp.* **34** 289 (1991)]
- Ivanitskii G R, Medvinskii A B, Tsyganov M A *Usp. Fiz. Nauk* **164** 1041 (1994) [*Phys. Usp.* **37** 961 (1994)]
- Dubey B, Das B, Hussain J *Ecolog. Model.* **141** 67 (2001)
- Wu Y, Zhao X *Physica D* **200** 325 (2005)
- Kuznetsov Yu A et al. *J. Math. Biol.* **32** 219 (1994)
- Kuznetsov Yu A et al. “Kross-diffuzionnaya model' dinamiki granitsy lesa” (“Cross-diffusion model of forest limit dynamics”), in *Problemy Ekologicheskogo Monitoringa i Modelirovaniya Ekosistem* Vol. 26 (St. Petersburg: Gidrometizdat, 1996) p. 213
- Burridge R, Knopoff L *Bull. Seismol. Soc. Am.* **57** 341 (1967)
- Cartwright J H E, Hernández-García E, Piro O *Phys. Rev. Lett.* **79** 527 (1997)
- Chaplain M A J, Stuart A M *IMA J. Math. Appl. Med. Biol.* **10** 149 (1993)
- Perumpanani A J, Sherratt J A, Norbury J *Nonlinearity* **10** 1599 (1997)
- Perumpanani A J, Byrne H M *Eur. J. Cancer* **35** 1274 (1999)
- Perumpanani A J, Norbury J *Math. Comp. Model.* **30** 123 (1999)
- Sherratt J A, Chaplain M A J *J. Math. Biol.* **43** 291 (2001)
- Marchant B P, Norbury J, Sherratt J A *Nonlinearity* **14** 1653 (2001)
- Jackson T L, Byrne H M *Math. Biosci.* **180** 307 (2002)
- Kolobov A V, Polezhaev A A, Solyanik G I *J. Theor. Med.* **3** 63 (2001)
- Romanovskii Yu M, Stepanova N V, Chernavskii D S *Matematicheskaya Biofizika* (Mathematical Biophysics) (Moscow: Nauka, 1984)
- Rubin A B *Biofizika* (Biophysics) 3rd ed. (Moscow: Izd. MGU, Nauka, 2004)
- Riznichenko G Yu *Lektsii po Matematicheskim Modelyam v Biologii* (Lectures on Mathematical Models in Biology) (Moscow-Izhevsk: RKhD, 2002)
- Svirezhev Yu M *Nelineinye Volny, Dissipativnye Struktury i Katastrofy v Ekologii* (Nonlinear Waves, Dissipative Structures, and Catastrophes in Biology) (Moscow: Nauka, 1987)
- Borisjuk G N et al. *Usp. Fiz. Nauk* **172** 1189 (2002) [*Phys. Usp.* **45** 1073 (2002)]
- Chernavskii D S *Usp. Fiz. Nauk* **170** 157 (2000) [*Phys. Usp.* **43** 151 (2000)]
- Shigesada N, Kawasaki K, Teramoto E *J. Theor. Biol.* **79** 83 (1979)
- Murray J D, Cohen J E R *SIAM J. Appl. Math.* **43** 66 (1983)
- Pettet G J, McElwain D L S, Norbury J *IMA J. Math. Appl. Med. Biol.* **17** 395 (2000)
- Chattopadhyay J, Chatterjee S *Nonlin. Phenom. Comp. Syst.* **4** 364 (2001)
- Murray J D, Deeming D C, Ferguson M W *Proc. R. Soc. London Ser. B* **239** 279 (1990)
- Murray J D, Myerscough M R *J. Theor. Biol.* **149** 339 (1991)
- Myerscough M R, Maini P K, Painter K J *Bull. Math. Biol.* **60** 1 (1998)
- Painter K J, Maini P K, Othmer H G *Proc. Natl. Acad. Sci. USA* **96** 5549 (1999)
- Painter K J “Modeling of pigment patterns in fish”, in *Mathematical Models for Biological Pattern Formation Frontiers in Biological Mathematics* (The IMA Volumes in Mathematics and its Applications, Vol. 121, Eds P K Maini, H G Othmer) (Berlin: Springer, 2001) p. 59
- Lauffenburger D A, Kennedy C R *J. Math. Biol.* **16** 141 (1983)
- Vasiev B N, Hogeweg P, Panfilov A V *Phys. Rev. Lett.* **73** 3173 (1994)
- Höfer T, Sherratt J A, Maini P K *Physica D* **85** 425 (1995)
- Marée A F M, Panfilov A V, Hogeweg P *J. Theor. Biol.* **199** 297 (1999)
- Marée A F M, Panfilov A V, Hogeweg P *Proc. R. Soc. London Ser. B* **266** 1351 (1999)
- Zhabotinskii A M *Kontsentratsionnye Avtokolebaniya* (Concentration Auto-Oscillations) (Moscow: Nauka, 1974)
- Vasil'ev V A, Romanovskii Yu M, Yakhno B G *Avtovolnovnye Protssesy* (Autowave Processes) (Moscow: Nauka, 1987)
- Kerner B S, Osipov V V *Avtosolitony* (Autosolitons) (Moscow: Nauka, 1991) [Translated into English (Dordrecht: Kluwer Acad., 1994)]
- Zhabotinskii A M et al. *Oscillations and Traveling Waves in Chemical Systems* (Eds R Field, M Burger) (New York: Wiley, 1985) [Translated into Russian (Moscow: Mir, 1988)]
- Krinskii V I, Mikhailov A S *Avotovolny* (Autowaes) (Novoye v Zhisni, Nauke i Tekhnike. Fizika (News in Life, Science and Technique. Physics) Issue 10) (Moscow: Znanie, 1984)
- Ataullakhanov F I et al. *Usp. Fiz. Nauk* **172** 671 (2002) [*Phys. Usp.* **45** 619 (2002)]
- Ivanitskii G R et al. *Biofizika* **33** 372 (1988)
- Agladze K I et al., in *Irreversible Processes and Selforganization* (Teubner-Texte zur Physik, Bd. 23, Eds W Ebeling, H Ulbricht) (Leipzig: BSB B.G. Teubner Verlagsgesellschaft, 1989) p. 34
- Agladze K et al. *Proc. R. Soc. London Ser. B* **253** 131 (1993)
- Tsyganov M A et al. *Dokl. Ross. Akad. Nauk* **333** 532 (1993) [*Dokl. Biophys.* **331/333** 100 (1993)]
- Tsyganov M A et al. *Phys. Rev. Lett.* **91** 218102 (2003)
- Tsyganov M A et al. *Physica D* **197** 18 (2004)
- Biktashev V N et al. *Chaos* **14** 988 (2004)
- Tsyganov M A, Biktashev V N *Phys. Rev. E* **70** 031901 (2004)
- Biktashev V N, Tsyganov M A *Proc. R. Soc. London Ser. A* **461** 3711 (2005)
- Brindley J, Biktashev V N, Tsyganov M A *Biol. Invasions* **7** 807 (2005)
- Adler J *Science* **153** 708 (1966)
- Adler J J. *Bacteriol.* **92** 121 (1966)

76. Tso W W, Adler J J. *Bacteriol.* **118** 560 (1974)
77. Taylor B L, Zhulin I B, Johnson M S. *Annu. Rev. Microbiol.* **53** 103 (1999)
78. Alexandre G, Greer-Phillips S, Zhulin I B. *FEMS Microbiol. Rev.* **28** 113 (2004)
79. Senina I N, Tyutyunov Yu V. *Zh. Obshch. Biol.* **63** 494 (2002)
80. Govorukhin V N, Morgulis A B, Tyutyunov Yu V. *Dokl. Ross. Akad. Nauk* **372** 730 (2000) [*Dokl. Math.* **61** 420 (2000)]
81. Arditi R et al. *Theor. Popul. Biol.* **59** 207 (2001)
82. Tyutyunov Yu, Senina I, Arditi R. *Am. Naturalist* **164** 722 (2004)
83. Flierl G et al. *J. Theor. Biol.* **196** 397 (1999)
84. Kareiva P. *Nature* **326** 388 (1987)
85. Okubo A, Chiang H C. *Res. Popul. Ecol.* **16** 1 (1974)
86. Okubo A, Chiang H C, Ebbesmeyer C C. *Can. Entom.* **109** 149 (1977)
87. Berezovskaya F S, Karev G P. *Usp. Fiz. Nauk* **169** 1011 (1999) [*Phys. Usp.* **42** 917 (1999)]
88. Berezovskaya F S et al. *Dokl. Ross. Akad. Nauk* **365** 416 (1999) [*Dokl. Biol. Sci.* **365** 148 (1999)]
89. Budrene E O. *Biofizika* **33** 373 (1988)
90. Budrene E O, Berg H C. *Nature* **349** 630 (1991)
91. Budrene E O, Berg H C. *Nature* **376** 49 (1995)
92. Medvinsky A B et al. *Physica D* **64** 267 (1993)
93. Tsyganov M A et al. *Dokl. Ross. Akad. Nauk* **339** 109 (1994)
94. Brenner M P, Levitov L S, Budrene E O. *Biophys. J.* **74** 1677 (1998)
95. Tyson R, Lubkin S R, Murray J D. *Proc. R. Soc. London Ser. B* **266** 299 (1999)
96. Mittal N et al. *Proc. Natl. Acad. Sci. USA* **100** 13259 (2003)
97. Lobanov A I et al. *Mat. modelir.* **14** (10) 17 (2002)
98. Erban R, Othmer H S. *SIAM J. Appl. Math.* **65** 361 (2004)
99. Tsyganov M A, Ivanitskii G R. *Biofizika* (2006) (in press)
100. Ron I G et al. *Physica A* **320** 485 (2003)
101. Shapiro J A. *Annu. Rev. Microbiol.* **52** 81 (1998)
102. Ben-Jacob E. *Nature* **415** 370 (2002)
103. Ben-Jacob E. *Philos. Trans. R. Soc. London Ser. A* **361** 1283 (2003)
104. Ben-Jacob E et al. *Trends Microbiol.* **12** 366 (2004)
105. Armitage J P. *Adv. Microbiol. Physiol.* **41** 229 (1999)
106. Falke J J, Hazelbauer G L. *Trends Biochem. Sci.* **26** 257 (2001)
107. Korobkova E et al. *Nature* **428** 574 (2004)
108. Berg H C. *Philos. Trans. R. Soc. London Ser. B* **355** 491 (2000)
109. Berg H C. *Phys. Today* **53** (1) 24 (2000)
110. Berg H C. *Annu. Rev. Biochem.* **72** 19 (2003)
111. Fenchel T. *Science* **296** 1068 (2002)
112. Mazzag B C, Zhulin I B, Mogilner A. *Biophys. J.* **85** 3558 (2003)
113. Sourjik V, Berg H C. *Proc. Natl. Acad. Sci. USA* **99** 123 (2002)
114. Thar R, Kühl M. *Proc. Natl. Acad. Sci. USA* **100** 5748 (2003)
115. Maeda K et al. *J. Bacteriol.* **127** 1039 (1976)
116. Taylor B L, Koshland D E (Jr). *J. Bacteriol.* **123** 557 (1975)
117. Taylor B L et al. *J. Bacteriol.* **140** 567 (1979)
118. Blakemore R. *Science* **190** 377 (1975)
119. Frankel R B, Blakemore R P. *Bioelectromagnetics* **10** 223 (1989)
120. Frankel R B et al. *Biophys. J.* **73** 994 (1997)
121. Eisenbach M et al. *Bioelectrochem. Bioenerg.* **10** 499 (1983)
122. Plesset M S, Winet H. *Nature* **248** 441 (1974)
123. Woodward D E et al. *Biophys. J.* **68** 2181 (1995)
124. Keller E F, Segel L A. *J. Theor. Biol.* **30** 225 (1971)
125. Koshland D E (Jr). *Physiol. Rev.* **59** 811 (1979)
126. Rozenfeld A F, Albano E V. *Physica A* **266** 322 (1999)
127. Monetti R, Rozenfeld A, Albano E. *Physica A* **283** 52 (2000)
128. Droz M, Pekalski A. *Physica A* **298** 545 (2001)
129. Truscott J E, Brindley J. *Philos. Trans. R. Soc. London Ser. A* **347** 703 (1994)
130. Matthews L, Brindley J. *Dyn. Stab. Syst.* **12** 39 (1997)
131. Petrov V, Scott S K, Showalter K. *Philos. Trans. R. Soc. London Ser. A* **347** 631 (1994)
132. Kobayashi R, Ohta T, Hayase Y. *Phys. Rev. E* **50** R3291 (1994)
133. Kosek J, Marek M. *Phys. Rev. Lett.* **74** 2134 (1995)
134. Mornev O A et al. *Dokl. Ross. Akad. Nauk* **347** 123 (1996) [*Dokl. Biophys.* **346/348** 21 (1996)]
135. Aslanidi O V, Mornev O A. *Biofizika* **41** 953 (1996)
136. Aslanidi O V, Mornev O A. *Pis'ma Zh. Eksp. Teor. Fiz.* **65** 553 (1997) [*JETP Lett.* **65** 579 (1997)]
137. Aslanidi O V, Mornev O A. *J. Biol. Phys.* **25** 149 (1999)
138. von Oertzen A et al. *J. Phys. Chem. B* **102** 4966 (1998)
139. Rotermund H H et al. *Phys. Rev. Lett.* **66** 3083 (1991)
140. Argentina M, Coulet P, Mahadevan L. *Phys. Rev. Lett.* **79** 2803 (1997)
141. Argentina M, Coulet P, Krinsky V J. *Theor. Biol.* **205** 47 (2000)
142. FitzHugh R. *Biophys. J.* **1** 445 (1961)
143. Nagumo J, Arimoto S, Yoshizawa S. *Proc. IEEE* **50** 2061 (1962)
144. Guriya G T, Kiyatkin A B, Muller S. *Biofizika* **38** 463 (1993) [*Biophysics* **38** 461 (1993)]
145. Aliev R R, Vasiev B N. *Chaos, Solitons Fractals* **5** 439 (1995)
146. Aliev R R, Panfilov A V. *Phys. Rev. E* **52** 2287 (1995)
147. Lobanova E S, Ataullakhanov F I. *Phys. Rev. Lett.* **91** 138301 (2003)
148. Winfree A T. *Chaos* **1** 303 (1991)
149. Barkley D, Kevrekidis I G. *Chaos* **4** 453 (1994)
150. Biktashev V N, Holden A V. *Physica D* **116** 342 (1998)
151. Biktashev V N. *Phys. Rev. Lett.* **95** 084501 (2005)
152. Mornev O A et al. *Pis'ma Zh. Eksp. Teor. Fiz.* **77** 319 (2003) [*JETP Lett.* **77** 270 (2003)]
153. Sherratt J A et al. *Proc. R. Soc. London Ser. B* **269** 327 (2002)
154. Zaikin A N. *Fiz. Myst' Rossii* (1) 54 (1995)
155. Journé J J. *Theor. Biol.* **65** 133 (1977)
156. Satulovskiy J E. *J. Theor. Biol.* **183** 381 (1996)
157. Saito H et al. *Nature* **309** 757 (1984)
158. Yarden Y, Ullrich A. *Annu. Rev. Biochem.* **57** 443 (1988)
159. Carlson J M, Langer J S. *Phys. Rev. Lett.* **62** 2632 (1989)
160. Carlson J M, Langer J S, Shaw B E. *Rev. Mod. Phys.* **66** 657 (1994)
161. Samarskii A A, Gulina A V. *Chislennyye Metody Matematicheskoi Fiziki* (Numerical Methods of Mathematical Physics) (Moscow: Nauchnyi Mir, 2003)
162. Mimura M, Kawasaki K J. *Math. Biol.* **9** 49 (1980)
163. Byrne H M, Owen M R. *J. Math. Biol.* **49** 604 (2004)
164. Galiano G, Garzon M L, Jünger A. *Rev. Real Acad. Ciencias, Ser. A Mat.* **95** 281 (2001)
165. Chen L, Hsiao L, Li Y. *Commun. Math. Sci.* **1** 799 (2003)
166. Chen L, Jünger A. *SIAM J. Math. Anal.* **36** 301 (2004)
167. Barrett J W, Blowey J F. *Numer. Math.* **98** 195 (2004)
168. Talanov V I. *Dokl. Akad. Nauk SSSR* **258** 604 (1981) [*Sov. Phys. Dokl.* **26** 522 (1981)]
169. Talanov V I, in *Nelineinye Volny: Samoorganizatsiya* (Nonlinear Waves: Self-Organization) (Executive Eds A V Gapanov-Grekhov, M I Rabinovich) (Moscow: Nauka, 1983) p. 47